



HAL
open science

The 3'UTR-derived sRNA RsaG coordinates redox homeostasis and metabolism adaptation in response to glucose-6-phosphate uptake in *Staphylococcus aureus*

Emma Desgranges, Laura Barrientos, Lucas Herrgott, Stefano Marzi, Alejandro Toledo-Arana, Karen Moreau, François Vandenesch, Pascale Romby, Isabelle Caldelari

► To cite this version:

Emma Desgranges, Laura Barrientos, Lucas Herrgott, Stefano Marzi, Alejandro Toledo-Arana, et al.. The 3'UTR-derived sRNA RsaG coordinates redox homeostasis and metabolism adaptation in response to glucose-6-phosphate uptake in *Staphylococcus aureus*. *Molecular Microbiology*, 2022, 117 (1), pp.193-214. 10.1111/mmi.14845 . hal-03836042

HAL Id: hal-03836042

<https://hal.science/hal-03836042>

Submitted on 2 Nov 2022

HAL is a multi-disciplinary open access archive for the deposit and dissemination of scientific research documents, whether they are published or not. The documents may come from teaching and research institutions in France or abroad, or from public or private research centers.

L'archive ouverte pluridisciplinaire **HAL**, est destinée au dépôt et à la diffusion de documents scientifiques de niveau recherche, publiés ou non, émanant des établissements d'enseignement et de recherche français ou étrangers, des laboratoires publics ou privés.

The 3'UTR-derived sRNA RsaG coordinates redox homeostasis and metabolism adaptation in response to glucose-6-phosphate uptake in *Staphylococcus aureus*

Journal:	<i>Molecular Microbiology</i>
Manuscript ID	MMI-2021-18579.R1
Manuscript Type:	Research Article
Date Submitted by the Author:	08-Nov-2021
Complete List of Authors:	Desgranges, Emma; Centre National de la Recherche Scientifique, UPR9002 Barrientos, Laura; Centre National de la Recherche Scientifique, UPR9002 Herrgott, Lucas; Centre National de la Recherche Scientifique, UPR9002 Marzi, Stefano; Centre National de la Recherche Scientifique, UPR 9002 Toledo-Arana, Alejandro; Spanish Scientific Research Council, Instituto de Agrobiotecnología (IdAB) Moreau, Karen; Centre International de Recherche en Infectiologie, U1111 Vandenesch, François; Centre International de Recherche en Infectiologie, U1111 Romby, Pascale; Centre National de la Recherche Scientifique, UPR 9002 Caldelari, Isabelle; Centre National de la Recherche Scientifique, UPR9002
Key Words:	3'UTR derived sRNA, <i>Staphylococcus aureus</i> , redox homeostasis

1 **The 3'UTR-derived sRNA RsaG coordinates redox homeostasis and**
2 **metabolism adaptation in response to glucose-6-phosphate uptake in**
3 ***Staphylococcus aureus***

4
5
6
7
8
9 Emma Desgranges¹, Laura Barrientos¹, Lucas Herrgott¹, Stefano Marzi¹, Alejandro
10 Toledo-Arana², Karen Moreau³, François Vandenesch³, Pascale Romby¹ and Isabelle
11 Caldelari^{1*}

12
13
14
15 ¹Université de Strasbourg, CNRS, Architecture et Réactivité de l'ARN, UPR9002, F-
16 67000 Strasbourg, France.

17 ²Instituto de Agrobiotecnología (IdAB). CSIC-UPNA-GN, 31192-Mutilva, Navarra,
18 Spain.

19 ³CIRI, Centre international de Recherche en Infectiologie, Inserm, U1111, Université
20 Claude Bernard Lyon 1, CNRS, UMR5308, École Normale Supérieure de Lyon,
21 Hospices Civils de Lyon, Univ Lyon, F-69008, Lyon, France.

22
23
24
25 **Running title:** A 3' untranslated region-derived sRNA responds to Glucose 6-
26 phosphate

27
28
29 **Keywords:** 3'UTR derived sRNA, *Staphylococcus aureus*, redox homeostasis

30
31
32 *To whom correspondence should be addressed. Tel: 33(0) 388417068; Fax: 33(0)
33 388602218; Email: i.caldelari@ibmc-cnrs.unistra.fr

34

35

36 **SUMMARY (199/200 words)**

37

38 *Staphylococcus aureus* RsaG is a 3' untranslated region (3'UTR) derived sRNA from
39 the conserved *uhpT* gene encoding a glucose-6-phosphate (G6P) transporter
40 expressed in response to extracellular G6P. The transcript *uhpT-RsaG* undergoes
41 degradation from 5' to 3' end by the action of the exoribonucleases J1/J2, which are
42 blocked by a stable hairpin structure at the 5' end of RsaG, leading to its accumulation.
43 RsaG together with *uhpT* are induced when bacteria are internalized into host cells or
44 in presence of mucus-secreting cells. Using MS2 affinity purification coupled with RNA
45 sequencing, several RNAs were identified as targets including mRNAs encoding the
46 transcriptional factors Rex, CcpA, SarA and the sRNA RsaI. Our data suggested that
47 RsaG contributes to the control of redox homeostasis and adjusts metabolism to
48 changing environmental conditions. RsaG uses different molecular mechanisms to
49 stabilize, to degrade, or to repress translation of its mRNA targets. While RsaG is
50 conserved only in closely related species, the *uhpT* 3'UTR of the ape pathogen *S.*
51 *simiae* harbors a sRNA, whose sequence is highly different, and which does not
52 respond to G6P levels. Our results hypothesized that the 3'UTRs from UhpT
53 transporter encoding mRNAs could have rapidly evolved to enable adaptation to host
54 niches.

55

56

57

58

59

60

61

62 INTRODUCTION

63

64 *Staphylococcus aureus* is usually described as an extracellular opportunistic pathogen,
65 infecting a wide range of organs and tissues. However, it also invades and replicates
66 in various phagocytic or non-phagocytic host cells (Hamza and Li, 2014). To be
67 successful as a pathogen, this bacterium needs to adapt to the hostile environments
68 of the host and must acquire imposed nutrients for its survival. Consequently,
69 staphylococcal genome encodes several transporters for metabolites (sugars, metals,
70 amino-acids, etc...), which are often primordial for virulence. For instance, a mutant
71 strain deprived of the four glucose transporters (*glcA*, *glcB*, *glcC* and *glcU*) is avirulent
72 in a murine skin infection model (Vitko *et al.*, 2016).

73 Metabolic and virulence genes are tightly controlled by transcriptional factors
74 (TFs), two-component systems (TCS), metabolite-sensing proteins and regulatory
75 RNAs to adapt to various environmental situations (Villanueva *et al.*, 2018; Richardson,
76 2019). *S. aureus* possesses a plethora of TFs such as CcpA, CodY and Rex,
77 responding to diverse stimuli (for review see (Richardson, 2019). In response to
78 glucose, the catabolite control protein CcpA, activates glycolytic genes, represses
79 expression of genes, whose products act in TCA cycle, gluconeogenesis, and amino
80 acid catabolism (Seidl *et al.*, 2009). It mediates catabolic repression allowing bacteria
81 to use the preferred carbon source. Besides, CodY, sensing both branched amino
82 acids and GTP, represses genes involved in amino acid synthesis and secreted
83 virulence factors (Richardson, 2019). Furthermore, Rex is considered as the central
84 regulator of anaerobic metabolism and inhibits transcription of genes encoding
85 fermentative enzymes such as lactate dehydrogenase Ldh1 or alanine
86 dehydrogenase Ald1 under aerobic conditions (Pagels *et al.*, 2010). At high
87 NADH/NAD level, when Rex is inhibited, survival of *S. aureus* depends on a metabolic
88 switch to promote fermentation in response to NO or to face the aerobic low redox
89 potential of host cytosol (Croke *et al.*, 2013; Christmas *et al.*, 2019). While immune
90 radicals damage the terminal oxidase of the electron transport chain leading to the
91 disruption of redox homeostasis, *S. aureus* produces predominantly L or D-lactate as
92 defences. The three lactate dehydrogenases Ldh1, Ldh2 or Ddh generate
93 respectively L- or D-lactate from glucose fermentation and support NAD⁺ recycling.
94 Therefore, CcpA activates transcription of the key enzyme Ldh1 only if *rex* is repressed
95 (Croke *et al.*, 2013). In contrast, when bacteria are internalized and glucose

96 unavailable, Ldh1 is not active, and the amino acids are preferred as nutrients
97 reflecting the derepression of the CodY and CcpA regulons (Michalik *et al.*, 2017).
98 Alongside TFs, the staphylococcal core genome encodes 16 two component systems
99 (TCS), which sense and respond to diverse stimuli and to various metabolites or small
100 compounds (Villanueva *et al.*, 2018). **In glucose-limiting conditions, when *S. aureus***
101 **penetrates host cells, the bacteria could utilise cytosolic glucose-6-phosphate (G6P)**
102 **instead of glucose, whose uptake relies on the hexose phosphate antiporter UhpT.**
103 **Expression of *uhpT* is induced by the TCS HptRS, which senses extracellular G6P**
104 (see below, and Garzoni *et al.*, 2007; Park *et al.*, 2015; Yang *et al.*, 2016). The
105 response regulator HptR binds to a consensus sequence called HptR box, localized
106 between -67 and -96 before the beginning of the transcriptional start site of *uhpT* (Yang
107 *et al.*, 2016). The disruption of *hptRS operon* impairs survival into various host cells,
108 suggesting that sensing and uptake of G6P is critical for *S. aureus* virulence (Park *et*
109 *al.*, 2015).

110 Regulatory RNAs (sRNA) cooperate with TFs and TCSs to quickly adjust the
111 bacterial physiology to the surrounding conditions and especially to the availability of
112 carbon sources (Bobrovskyy and Vanderpool, 2013; Wagner and Romby, 2015;
113 Desgranges *et al.*, 2019). They often act at the post-transcriptional level and hybridize
114 to their mRNA targets through imperfect complementarities to regulate positively or
115 negatively their stability or translation. The vast majority of sRNAs derives from
116 intergenic regions (IGR) and possesses their own promoter, otherwise they are
117 processed from 5' or 3' untranslated regions (UTRs) of mRNAs (Miyakoshi *et al.*, 2015;
118 Desgranges *et al.*, 2019). Their transcription is often induced by sensing of external
119 stimuli via TCS or TF (Brosse and Guillier, 2018). The targetomes of different
120 staphylococcal sRNAs were identified and reflected the diversity of pathways in which
121 they intervene (e.g., Augagneur *et al.*, 2020; Bronesky *et al.*, 2019; Lalaouna *et al.*,
122 2019; Rochat *et al.*, 2018; Tomasini *et al.*, 2017). Several of them are part of large
123 regulatory networks that connect major regulatory proteins of virulence gene
124 expression (CodY, CcpA, SigB, AgrA, SrrAB) in response to wide arrays of metabolic
125 and environmental signals (Desgranges *et al.*, 2019). For instance, the sRNA RsaI is
126 repressed by CcpA in presence of glucose. When glucose decreases, RsaI
127 downregulates glucose uptake and activates fermentation, energy production, and NO
128 detoxification. RsaI binds to other sRNAs, such as RsaD, RsaE and RsaG (Bronesky
129 *et al.*, 2019). SrrA, which senses nitric oxide, activates RsaE to repress the synthesis

130 of many TCA enzymes, and to reduce NADH production. In turn, low activity of the
131 TCA cycle has a positive effect on the *agr* system to adjust virulence factor production
132 under stress conditions. Conversely, presence of NAD⁺ enhances binding of Rex to
133 RsaE promoter region to repress its expression (for a review, Marincola *et al.*, 2019).

134 Here we show that the 3'UTR-derived sRNA, RsaG, conserved in *S. aureus* and
135 in very close relative species, accumulates when G6P is available extracellularly. This
136 sRNA is derived from the degradation of *uhpT* mRNA encoding the hexose phosphate
137 antiporter UhpT. Using combination of approaches, we propose that RsaG contributes
138 to the regulation of redox homeostasis, and metabolism adaptation when G6P is
139 metabolized. The consequences of RsaG functions on *S. aureus* pathogenesis will
140 also be discussed.

141

142 RESULTS

143

144 RsaG expression is induced by G6P upon the *uhpT* promoter.

145 RsaG was first identified as an intergenic region that is conserved only in *S. aureus*
146 (Geissmann *et al.*, 2009). RsaG is located downstream the *uhpT* gene and was shown
147 to accumulate in the late exponential phase of growth in rich medium (Geissmann *et*
148 *al.*, 2009) or in presence of G6P (Bronsky *et al.*, 2019). Because no obvious predicted
149 promoter sequence was detected for *rsaG* and because *uhpT* is induced in response
150 to extracellular G6P (Bronsky *et al.*, 2019), we have revisited the mechanism leading
151 to the accumulation of RsaG.

152 We first tested RsaG expression by Northern blot analysis in MHB (Muller
153 Hinton Broth) with or without G6P in the wild-type (HG001) strain, the mutant strains
154 carrying either a deletion of the *hptRS* system (HG001 Δ *hptRS*) or a deletion of the
155 *uhpT* promoter containing the *hptR* box recognized by the transcriptional regulator
156 HptR (HG001 Δ *PuhpT*) (Figure 1A). In MHB, in which starch is added as carbon source,
157 RsaG is constitutively and weakly expressed. In contrast when the medium is
158 supplemented with G6P, we observed a large increase of RsaG transcription, which is
159 almost completely abolished in the HG001 Δ *hptRS* or HG001 Δ *PuhpT* mutant strains
160 (Figure 1A). Furthermore, we also detected bands with higher molecular weights
161 showing the presence of a longer transcript containing RsaG and corresponding to the
162 size of *uhpT* (1782 nucleotides). We then constructed various transcriptional fusions

163 carrying *gfp* in place of RsaG and determined the effect of successive deletions within
164 *uhpT* and its promoter on GFP synthesis (Figure 1B). All the constructs were
165 expressed from a plasmid that was transformed into HG001. **The data were analysed**
166 **by western blot using an anti-GFP antibody (Figure 1C). GFP bacteria were detected**
167 **only with *uhpT* full length containing its promoter and the *hptR* box.**

168 Taken together, these data evoked that RsaG is mainly transcribed together
169 with *uhpT* under the control of the same promoter responding to G6P via HptRS, and
170 that RsaG accumulated most probably after a rapid degradation of *uhpT* mRNA.

171

172 **The *uhpT* mRNA and RsaG are enhanced under conditions mimicking infection.**

173 G6P is the activated form of glucose in numerous cellular metabolic pathways and
174 hexose-phosphate sugars are predominant in the cytosolic environment (Chico-Calero
175 *et al.*, 2002). Upon internalization into host cells, *S. aureus* senses cytosolic G6P and
176 may consume it as a carbon source. We first compared the growth rate of HG001,
177 HG001 Δ *rsaG*, and HG001 Δ *hptRS* strains in glucose depleted LB medium or in
178 presence of 0,5 % G6P. **Without G6P, the three strains grew equally. In contrast, the**
179 **wild type HG001 strain and the Δ *rsaG* deletion mutant grew faster in presence of G6P**
180 **than the HG001 Δ *hptRS* strain under identical conditions** (Figure 2A). These data
181 indicated that RsaG is not required for G6P catabolism **in contrast to the TCS HptRS.**
182 We **next** performed internalization assays with HG001 and HG001 Δ *hptRS* strains in
183 (non-phagocytic) myoblasts and (phagocytic) macrophages cell lines cultured in K-
184 MEM or D-MEM medium, respectively. Quantification of RsaG levels in intracellular
185 bacteria was monitored by qRT-PCR. The data showed that RsaG is induced 100-fold
186 under these conditions and that the activation is dependent of HptRS, which allows the
187 expression of the *uhpT*-*RsaG* co-transcript (Figures 2B and S1A).

188 Because *S. aureus* is primarily an extracellular pathogen, we postulated that
189 bacteria might face G6P in contact with host cells producing mucus either in intestine
190 or lungs. **Four days-cultivated A549 airway epithelial cells, which produce high levels**
191 **of mucin as measured with two different antibodies MUC-5AC and MUC-2 (Figure 2C,**
192 **right panel), were incubated with the HG001 and HG001 Δ *hptRS* strains. Bacteria were**
193 **gently recovered, and total RNA was extracted. Northern blot experiments were**
194 **performed with a probe specific for RsaG. The data showed that expression of RsaG**
195 **and of a higher band corresponding to *uhpT*-*RsaG* transcript was highly induced when**

196 HG001 was mixed with A549 cells in contrast to HG001 incubated with liver HU-H7
197 cells that do not synthesize mucin (Figure 2C, left panel). This effect is strictly
198 dependent on the TCS HptRS since no significant signal was observed for RsaG in
199 the mutant strain HG001 Δ *hptRS*. We also compared the accumulation of RsaG when
200 staphylococci were incubated in presence of colon cell lines HT-29 or HT-29MTX
201 cultivated for 4 days and for 14 days to allow differentiation and production of mucus
202 (Figure S1B, right panel) (von Kleist *et al.*, 1975; Behrens *et al.*, 2001). HT-29 cells are
203 heterogeneous cells as they contain less than 5% of mucus-secreting cells. HT29-MTX
204 cells have been obtained from HT-29 cultures after treatment with methotrexate, to
205 give more homogeneous and stable mucus-secreting cells. A strong induction of RsaG
206 was observed when HG001 strains were incubated with either HT-29 or HT-29 MTX
207 cells cultivated for 14 days as compared to HG001 strains incubated with either HT-29
208 or HT-29 MTX cells cultivated for 4 days, respectively (Figure S1B). This effect is linked
209 to G6P entry because RsaG accumulation was no more observed when the mutant
210 strain HG001 Δ *hptRS* was incubated with HT-29 and HT-29 MTX cells (Figure S1B).

211 In summary, we defined two different environmental conditions in which *uhpT*
212 mRNA and consequently RsaG are induced. Because RsaG is not essential for growth
213 in the presence of G6P, we proposed that RsaG is not required for G6P uptake and
214 catabolism but might contribute to adapt the cells in new environments during the
215 infection, i.e. presence of mucus and/or internalization into host cells.

216

217 **RsaG is derived from the maturation of the 3'UTR of *uhpT*.**

218 Because only primary transcripts have triphosphates at the 5' end, we used the 5'-
219 phosphate-dependent exonuclease Terminator™ (Tex) to discriminate the
220 phosphorylation status of the 5' end of RsaG. Total RNAs extracted from HG001 grown
221 in BHI for 4 h (when RsaG is present) was treated with or without Tex and run on an
222 agarose gel. Surprisingly, RsaG level was only slightly reduced in presence of Tex
223 (Figure 3A, left panel). This result might be due to the fact that the activity of Tex is
224 altered by the presence of a helical structure present at the 5' end, as found for 5S
225 rRNA, which is also resistant to Tex treatment (Figure 3A, right panel). A longer
226 exposition of the autoradiography showed that the *uhpT-rsaG* transcript and shorter
227 fragments were digested by Tex (Figure S2A). However, a faint band can still be
228 observed at the top of the gel in treated samples, which could correspond to the 5'-
229 triphosphate *uhpT-RsaG* transcript, which is not fully degraded. As positive controls,

230 ethidium bromide staining revealed that the bulk 16S and 23S rRNAs (carrying a
231 monophosphate at their 5' ends) were fully degraded by Tex (Figure 3B, left panel). In
232 contrast, Northern blot analysis showed that the *bona fide* sRNA RsaI (containing a 5'-
233 triphosphate end) was resistant to Tex (Figure 3B, right panel). These data suggested
234 that the degradation process of the long *uhpT* transcript involves a 5' exoribonuclease,
235 which would be partially blocked by the 5' stem-loop structure of RsaG.

236 In the following experiments, we have tested the involvement of the major
237 ribonucleases from *S. aureus*, namely RNase P, RNase III, RNases J1/J2 and RNase
238 Y (Figures 3C and S2B, C and D). An *in vitro* transcribed *uhpT-rsaG* RNA was used in
239 the assay with the RNA component of RNase P, which is sufficient to induce cleavage
240 (Guerrier-Takada and Altman, 1984). The data showed that the co-transcript was not
241 cleaved in contrast to the pre-mature tRNA, which was used as a positive control
242 (Figure S2B). For the other enzymes, Northern blot experiments were performed on
243 total RNAs prepared from various mutant strains carrying deletion at specific genes
244 encoding RNase III (HG001 Δrnc), RNase Y (HG001 Δrny), and RNases J1 or J2
245 (RN4220 $\Delta j1$, Sa624 $\Delta j1$ or Sa624 $\Delta j2$), and their parent wild-type strains (HG001,
246 RN4220 or Sa624). The strains were grown in MHB containing G6P, and RsaG was
247 revealed using a specific probe. While RNase Y and RNase III did not significantly alter
248 the maturation of *uhpT*-RsaG transcript (Figure S2C), a significant decrease of RsaG
249 level was observed in the single deletion mutants of either RNase J1 ($\Delta j1$) or RNase
250 J2 ($\Delta j2$), and concomitantly an accumulation of *uhpT*-RsaG was visualized (Figures
251 3C and S2D). Because the growth of the double mutant strain ($\Delta j1\Delta j2$) was strongly
252 impaired, we did not manage to obtain enough bacteria to extract sufficient amount of
253 RNAs for further analysis (Linder *et al.*, 2014). In the mutant $\Delta j1$ and $\Delta j2$ strains, the
254 size of RsaG appears to be slightly longer than in the parental WT strain suggesting
255 that the J1/J2 heterodimer is required for RsaG complete maturation (Figures 3C and
256 S2B).

257 Taken together the data strongly suggested that RsaG is a product of the rapid
258 degradation of the full-length *uhpT* mRNA and involves the 5'-3' exoribonuclease
259 activities of RNases J1/J2 (Figure 3D), which are both able to degrade mono- or
260 triphosphate 5' end of transcripts (Linder *et al.*, 2014). The 5' hairpin structure of RsaG
261 (Figure 4A) most probably blocks the progression of the exoribonucleases.

262

263 **Defining the RsaG targetome.**

264 In order to identify RsaG functions, the MAPS approach (“MS2 affinity purification
265 coupled to RNA sequencing”) was applied to identify the RsaG targetome (Lalaouna
266 *et al.*, 2018a). Briefly, the MS2 tagged version of RsaG was expressed from a plasmid
267 under the control of the P3 promoter in the Δ rsaG mutant strain. To mimic the inducible
268 conditions of RsaG, the growth was performed for 5 h in BHI medium and then G6P
269 0,5 % was added for 1 h before harvesting. As controls, we showed that the MS2-
270 RsaG is specifically retained by the column (Figure S3A) and is as stable as the
271 chromosomal copy (Figure S3B). After elution and extraction, RNAs were sequenced,
272 and the data were analysed using **the tools of Galaxy platform (<https://usegalaxy.org/>)**
273 (Afgan *et al.*, 2016). The sequencing reads were mapped, counted per feature, and
274 normalized using the HG001 genome as previously described (Tomasini *et al.*, 2017).
275 The enrichment of putative RsaG targets was derived by comparison of the number of
276 reads obtained from the MS2-RsaG purification and the MS2 alone as control. In the
277 latter case, the MS2 tag alone was expressed in the wild-type HG001 strain. We have
278 considered as RsaG targets, the RNAs that were enriched at least two-fold and were
279 reproducibly and significantly detected in two independent experiments (Table S1).

280 Among the most enriched RNAs, we identified several mRNAs encoding
281 transcriptional regulatory proteins (SarA, SlyA, SarX, SarV, Rex, TcaR, CcpA, RpiR).
282 In addition, the PTS operon (phosphoenolpyruvate (PEP)-dependent
283 phosphotransferase system) encoded the genes *ptsH* and *ptsI*, allows carbohydrates
284 transport and phosphorylation before entry into glycolysis. **G6P promotes the
285 phosphorylation and activation of the histidine-containing phosphocarrier protein HPr,
286 encoded by *ptsH*, which is the activator of CcpA. Hence HPr connects glycolytic activity
287 with carbon catabolite repression (Deutscher *et al.*, 1995). Other metabolic operons
288 were also enriched** including the *arcABDCR* operon, which is involved in arginine
289 catabolism when *S. aureus* grows in anaerobic conditions (Makhlin *et al.*, 2007), the
290 *Thi* operon required for thiamine biosynthesis, an indispensable cofactor of enzymes
291 involved in amino acid and carbohydrate metabolism, and various dehydrogenases
292 (Ald2, Ndh, Hom). Besides, we have pulled out several polycistronic transcripts
293 encoding transporters including the mechanosensitive ion channel MscL, the ABC
294 transporters for K⁺ and Mn²⁺. KdpBAF and MntABC, respectively (Xue *et al.*, 2011;
295 Ando *et al.*, 2003), the *Pmt* operon that exports the PSM toxins (phenol soluble
296 modulins) causing host cell lysis (Chatterjee *et al.*, 2013), and the multi-drug efflux

297 pumps SrdM-SepA. Finally, although RsaI is weakly expressed in presence of G6P, it
298 is among the best candidates enriched with RsaG (Bronesky *et al.*, 2019). We also
299 considered the two poorly enriched *ldh1* and *fn3k* mRNAs because *ldh1* encoding
300 lactate dehydrogenase is repressed by Rex and activated by CcpA, while *fn3k*
301 translation is repressed by RsaI (Table S1) (Bronesky *et al.*, 2019).

302 We then verified that RsaG is able to form stable complexes with 39 co-purified
303 RNAs. Gel retardation assays were performed with a 5' end labeled RsaG incubated
304 with increasing amounts of the potential target RNAs. The data showed that the
305 majority of mRNA candidates (28 out of 39) formed stable basepairings with RsaG with
306 binding affinities ranging from 50 nM to 600 nM (Table S1, Figures 4A and S4). The
307 binding strength was not correlated with the enrichment factors since the poorly
308 enriched mRNAs *ldh1* and *fn3k* form also stable complexes with RsaG (Table S1).
309 Eleven RNAs were not able to form stable complexes with RsaG *in vitro*, and among
310 them, *glcU_2* and the hypothetical proteins HG001_02010, HG001_02210 and
311 HG001_02520 were shown to be direct targets of the sRNA RsaI (Bronesky *et al.*,
312 2019). These mRNAs were most probably pulled down with RsaI since their binding
313 sites are different from RsaG (Bronesky *et al.*, 2019). Surprisingly, among the first 20
314 most enriched candidates, four mRNAs (*mscL*, *cspA*, *slyA_2* and *arcC2*) did not
315 interact efficiently with RsaG *in vitro* (Table S1, Figures S4). Most probably that *arcC2*
316 was pulled down together with *arcR* as both genes are located on the same operon.
317 For the other mRNAs, either the structure of the full-length mRNAs was not correctly
318 folded *in vitro* or that an unknown trans-acting factor might be required *in vivo* to
319 promote complex formation.

320 The MAPS data did not reveal any mRNAs involved directly in the G6P
321 catabolism supporting the hypothesis that RsaG would adapt the bacterial metabolism
322 in response to G6P uptake.

323

324 **RsaG hinders ribosome binding on several mRNA targets.**

325 Among the top 20 candidates, stable basepairing interactions between RsaG and the
326 ribosome binding site (RBS) of several mRNAs were predicted using CopraRNA and
327 IntaRNA (Wright, *et al.*, 2014), i.e, *ccpA*, *sarA*, *arcR*, *tcaR*, *ndh*. Likewise, RsaG is
328 predicted to interact with the 5'UTR of several mRNAs, i.e, *sarX*. The C-rich sequence
329 in the interhelical region (C90-C92) of RsaG is complementary to the SD sequences
330 of mRNAs encoding the biofilm repressor TcaR (Brandenberger *et al.*, 2000; Jefferson

331 *et al.*, 2004) and the accessory regulator SarA (Cheung *et al.*, 2008), while the nts 126
332 to 148 of RsaG are complementary to the RBS of *ccpA* mRNA encoding the catabolite
333 control protein A (Seidl *et al.*, 2009) (Figures 4A). RsaG binds efficiently to *tcaR*, *sarA*,
334 and *ccpA* mRNAs (Figure 4B). Base substitutions in one of the C-rich motifs of RsaG
335 (RsaG mut1, RsaG mut2) did not significantly alter the binding of RsaG mutants to
336 *tcaR* and *sarA* mRNAs, but a noticeable effect on binding efficiency was observed with
337 the double mutant RsaG mut1/2 (Figure S5). Due to the presence of three redundant
338 C-rich sequence motifs in RsaG, alternative pairings are possible (Figure 4A).

339 The consequence of the SD sequestration by RsaG on the formation of the
340 initiation ribosomal complex was then addressed by toe-printing assays with *tcaR*, *sarA*
341 and *ccpA* mRNAs (Figure 4C). For the three mRNAs, the addition of the initiator
342 tRNA^{Met} and of the *S. aureus* 30S subunits causes a pause of the reverse transcriptase
343 at position +16, the so-called toe-print. The addition of increasing concentrations of
344 RsaG strongly decreased the toe-print signal showing that RsaG is able to prevent the
345 formation of the initiation ribosomal complexes. Hence, RsaG might act as a
346 translational repressor. However, using antibodies against CcpA or against a flag-
347 tagged SarA, we did not detect significant changes of the protein yields in the WT and
348 mutant Δ *rsaG* strains grew in the presence of G6P (results not shown). The
349 discrepancy between the *in vitro* and *in vivo* data suggested a possible hierarchical
350 regulation of the targets *in vivo*.

351
352 **RsaG differentially alters the mRNA stabilities of *rex* and its regulated target *ldh1***

353 The mRNA encoding the redox transcriptional repressor Rex was highly enriched with
354 RsaG in MAPS. Basepairings were predicted between RsaG and several distant
355 regions of *rex* (Figures 5A et 5B). The 5' end of *rex* (nts -105 to -98) can form several
356 basepairings with nts 117 to 138 of RsaG (C site, Figure 5A). Besides alternative
357 interactions are predicted to occur between either the apical loop (nts 41 to 49, A site)
358 or nts 102 to 117 (B site) of RsaG with the *rex* coding sequence (nts 185-194) (Figure
359 5A). Based on these predictions, we have constructed two RsaG mutants carrying
360 base substitution (RsaG mut3, RsaG mut4) to alter the A and B binding sites,
361 respectively. *In vitro* binding assays showed that RsaG formed a stable complex with
362 *rex* mRNA (around 150 nM), and that only mutation in the B region of RsaG completely
363 eliminate the binding to *rex* mRNA (Figure 5B). We also introduced R2 substitutions
364 (Figure 5A) in the *rex* coding region, which partially restore basepairing

365 complementarity with RsaG mut3 or RsaG mut4. As expected, RsaG cannot bind to
366 *rex* containing the R2 substitution, but surprisingly, neither RsaG mut3 nor RsaG mut4
367 compensate the R2 mutations in *rex* mRNA (Figure 5B). Lead-induced cleavage was
368 performed to monitor the effect of *rex* mRNA binding on 5' end labeled RsaG (Figure
369 S6B). Significant reduced cleavages were observed in the 5' hairpin loop (nts 40 to 51)
370 and in the interhelical region (nts 98 to 110) of RsaG (Figure S6B). Although we did
371 not manage to find appropriate mutations to fully characterize the basepairing schemes,
372 our data strongly suggested that complex formation involves two distant regions of
373 both RNAs.

374 Based on these data, we cloned *rex* mRNA including the whole 5' UTR (103
375 nts) and 207 nts of its coding sequence in frame with *lacZ* under the control of the
376 strong promoter *PrpoB* and *rsaG* was cloned under the constitutive *blaZ* promoter. The
377 synthesis of β -galactosidase was analyzed in the Δ *rsaG* mutant strain transformed with
378 the plasmid carrying the *lacZ* reporter alone or with the plasmid containing the *lacZ*
379 and *rsaG*. The β -galactosidase activity was reproducibly increased by two-fold in cells
380 expressing RsaG (Figure S6C). Because RsaG binds to the 5' end of *rex* and to a
381 hairpin region, which partially sequesters the SD sequence, we wondered whether
382 RsaG might facilitate ribosome recruitment on *rex* mRNA. However, using Toe-printing
383 assays, the addition of increasing concentrations of RsaG did not enhance the
384 formation of the ternary ribosomal complex including *rex* mRNA, the initiator tRNA and
385 the 30S subunit (Figure S6D). We then analysed whether RsaG might impact *rex*
386 mRNA stability. Using rifampicin assays, the half-life of *rex* mRNA was measured in
387 the WT strain HG001, the deleted strain of *rsaG* (HG001 Δ *rsaG*) grown in presence or
388 absence of G6P, and in the deleted strain of *rsaG* complemented with a plasmid over-
389 expressing RsaG under the P3 promoter (HG001 Δ *rsaG* pCN51::P3*rsaG*). In absence
390 of G6P, the half-life of *rex* mRNA was less than 30 sec in the WT and Δ *rsaG* mutant
391 strains while the overexpression of RsaG in the mutant strain enhanced the half-life to
392 90 sec (Figure 5C). In presence of G6P, the half-life of *rex* reached values above 1
393 min in the WT strain (77.9 sec) and in the mutant strain overexpressing RsaG while
394 *rex* was poorly detected in the mutant Δ *rsaG* strain (Figures 5C and S6A). These data
395 suggested that enhancing the yield of RsaG stabilizes *rex* mRNA. Because *rex* mRNA
396 presented several hairpin structures in the 5' end, we analyzed whether the
397 endoribonuclease III might be involved in the degradation pathway of the mRNA. In
398 the absence of G6P, the half-life of *rex* mRNA was indeed enhanced two fold as

399 compared to the WT strain, and this effect was independent of the accumulation of
400 RsaG (Figure S6E).

401 Interestingly the main repressed target of Rex, the lactate deshydrogenase
402 Ldh1 was found in MAPS albeit with a threshold below 2-fold. Therefore, RsaG would
403 act on *ldh1* expression either directly or indirectly through the stabilisation of *rex* mRNA.
404 Prediction of pairing between *ldh1* and RsaG indicated that the large interhelical
405 unpaired region (nts 88 to 109) of RsaG might form basepairings with the RBS of *ldh1*
406 mRNA with the SD (-14 to +2) and with its coding region (+15 to +20) (Figure 6A).
407 Base substitution of the second C-rich motif of RsaG (RsaG mut2) did not impair
408 binding with *ldh1* most probably due to the formation of alternative pairings involving
409 the other C-rich motifs. Because we failed to design mutations that disrupt *ldh1* mRNA-
410 RsaG pairings, an indirect approach based on competition experiment was performed
411 using a single strand DNA oligonucleotide complementary to 34 nucleotides of *ldh1*
412 mRNA (from -14 to +20). Using gel retardation assay, this probe was sufficient to
413 compete efficiently with the mRNA (Figure 6B). Surprisingly, using Toe-printing assays,
414 RsaG binding to *ldh1* mRNA had only minor effect on the formation of the ternary
415 ribosomal complex (Figure S7A). The stability of *ldh1* mRNA was measured using
416 rifampicin treatment after 4 h of growth in absence or presence of G6P from HG001
417 strain and from the Δ *rsaG* deleted strain complemented with a vector expressing RsaG.
418 Quantification of the data revealed that the half-life of *ldh1* was strongly decreased
419 from around 10 min to 2-3 min when RsaG expression was strongly induced (Figure
420 6C).

421 Our data suggested that RsaG acts as a post-transcriptional regulator to
422 modulate positively or negatively the stability of target mRNAs. Through the regulation
423 of *rex* and *ldh1*, RsaG would avoid glycolytic fermentation in favour of amino acid
424 catabolism, when G6P is consumed.

425

426 **RsaI interferes with the binding of specific targets of RsaG.**

427 We previously identified that the second G-rich (nts 20-23) motif of RsaI binds to RsaG
428 (Figure 7). Binding of RsaG did not prevent RsaI to interact with its target mRNA
429 *glcU_2* (Bronesky *et al.*, 2019). Using base substitutions in RsaG, we could decipher
430 that only the C-rich motif in the apical loop of RsaG (nts 46-48) forms stable
431 basepairings with RsaI *in vitro* (Figures 7A, 7B). The consequence of RsaG-RsaI
432 interaction on several RsaG targets recognition was then monitored by gel retardation

433 assays. Radiolabeled RsaG was mixed together with *sarA* mRNA at a concentration
434 sufficient to bind most of RsaG molecules. The addition of increasing amount of RsaI
435 induces the appearance of a supershift indicating the formation of a ternary complex
436 RsaI-RsaG-*sarA* (Figure 7C). Conversely, when the same experiment was performed
437 between RsaG, RsaI, and *rex* or *steT* mRNAs, a competition was clearly observed
438 (Figures 7D, 7E). These data are well correlated with the fact that *sarA* and RsaI bind
439 to two distinct regions of RsaG while RsaI, *steT*, and *rex* have overlapping interaction
440 sites.

441 In the list of targets enriched by MAPS, we identified several potential targets
442 common to both RsaI and RsaG, *i.e.* *glcU_2*, *icaR*, HG001_02210 and HG001_02520,
443 *tdcB*, *treB* and *fn3K* (Table S1). Most of them did not bind directly to RsaG *in vitro*
444 (except *fn3k*, *treB* and *tdcB*) and no significant basepairing sites were predicted
445 suggesting that they were purified through RsaI (Figure S4). For *fn3K*, RsaI was
446 described as a translational repressor since the interaction site covered the RBS
447 (Bronesky *et al.*, 2019). In contrast, the second C-rich motif (nts 90 to 93) of RsaG
448 interacted within the *fn3K* coding region (Figure S7B). Indeed, gel retardation assays
449 showed that the 5' end labeled RsaG did not hybridize to an *in vitro* transcribed RNA
450 corresponding to the 5' UTR of *fn3K* but was able to form a stable complex with an *in*
451 *vitro* transcribed RNA including the open reading frame of *fn3K* (Figure S7B). The
452 result was further validated using competition experiments with an oligonucleotide of
453 17 nucleotides (nts 268 to 285 complementary to *fn3k*), which efficiently competes with *fn3K*
454 to bind RsaG *in vitro* (Figure S7B). The stability of *fn3k* mRNA was measured using
455 rifampicin treatment after 4 h of growth. Total RNAs were extracted from HG001 strain
456 in absence or presence of G6P, and the Δ *rsaG* deleted strain complemented with a
457 vector expressing RsaG. The data showed that the expression of RsaG significantly
458 destabilizes *fn3K* as the half-life decreases from 4 min to 2 min (Figure 6C). Another
459 common target between RsaG and RsaI is *tdcB* mRNA whose predicted binding sites
460 are different. Gel retardation assays performed with 5' end labeled RsaG mixed
461 together with *tdcB* mRNA and an increasing amount of RsaI showed a supershift
462 indicating the formation of a ternary complex RsaI-RsaG-*tdcB* (Figure 7F).

463 In summary, RsaI affects the binding of only part of RsaG mRNA targets.

464

465 **Differential evolution of the *uhpT* 3'UTRs containing RsaG in *Staphylococcaceae*.**

466 The *uhpT* gene sequence is highly conserved in the *Staphylococcaceae* family
467 (between 83 to 91% similarity). However, previous studies indicated that RsaG was
468 only conserved in *S. aureus* (Geissmann et al., 2009). Since we have demonstrated
469 that RsaG is derived from the long *uhpT* 3'UTR, we analyzed the *uhpT-rsaG-hptRS*
470 locus conservation among *Staphylococcus* species using Blastn. The results showed
471 that *hptRS* genes on the complementary strand were conserved as well as *uhpT*
472 (Figure 8A). In contrast, the *uhpT* 3'UTR containing RsaG appears to be only
473 conserved in *S. argenteus* and *S. schweitzeri*, which are closely related to *S. aureus*,
474 while the sequence and the size considerably diverged in *S. epidermidis* and *S. simiae*
475 (Figure 8A). This was in agreement with previous results that showed an evolutionary
476 bias within *Staphylococcus* 3'UTRs (Menendez-Gil et al., 2020).

477 Using a specific probe against *S. aureus* RsaG sequence, we identified a
478 transcript in *S. argenteus* and *S. schweitzeri* from total RNAs extracted from bacteria
479 cultures performed in the presence of G6P. Hence, RsaG is also produced in these
480 species despite some nucleotide differences (Figure 8B). In contrast, using a specific
481 *S. epidermidis* RsaG probe, we were unable to detect a processed 3'UTR from *uhpT*
482 mRNA in *S. epidermidis*, even if *uhpT* mRNA was weakly expressed in presence of
483 G6P since the mRNA was only detected by RT-PCR. Interestingly, when using a
484 specific probe against *S. simiae* 3'UTR, a signal corresponding to a larger processed
485 3'UTR was visualized (Figure 8B). The 5'-end of the processed band was then
486 determined using reverse transcription assays with total RNAs extracted from *S.*
487 *simiae* cultures (Figure 8C). The 5'-end localized 195 bp downstream of the stop codon
488 of *uhpT* resulting to an apparent 3'UTR derived sRNA of 726 nts in *S. simiae*, which
489 was significantly larger in comparison to *S. aureus* (294 nts). As the HptR box is rather
490 conserved, the induction of the orthologous *S. simiae* RsaG in absence or presence of
491 G6P was analyzed (Figure 8D). Unexpectedly, the accumulation of the 3'UTR was
492 independent of the presence of G6P. Although the sequence of the 3'UTR of *S. simiae*
493 *uhpT* has diverged, the maturation process might be conserved. Prediction of the
494 secondary structure of *S. simiae* RsaG revealed a hairpin structure at its 5' end, which
495 might block the progression of RNases J1/J2.

496

497 DISCUSSION

498 In this study, we have identified RsaG as a new 3' UTR-derived sRNA
499 processed from *uhpT* mRNA encoding the transporter of G6P. The transcription of

500 *uhpT* is activated by the TCS HptRS, which senses the external concentration of G6P.
501 In *S. aureus*, G6P is critical when the bacteria is internalized into host cells because a
502 mutant strain deprived of *hptRS* is not able to survive (Park *et al.*, 2015). However,
503 RsaG is not essential for growth when G6P is used as the solely carbon source. We
504 also showed that *uhpT* mRNA and RsaG are highly induced by G6P when *S. aureus*
505 is internalised into host cytosol and in presence of pulmonary or intestinal mucus
506 (Figure 2; Garzoni *et al.*, 2007). Our data suggested that RsaG might expand the action
507 of HptRS/UhpT by fine-tuning the cell metabolism in response to G6P uptake. RsaG
508 is different from *E. coli* SgrS, which protects the cell against glucose-phosphate stress
509 and from the depletion of glycolytic intermediates (Richard *et al.*, 2013). Interestingly,
510 a hierarchical regulation mediated by SgrS has been demonstrated (Bobrovskyy *et al.*,
511 2019; Poddar *et al.*, 2021). At low level, SgrS represses *ptsG*-encoded glucose
512 transporter, and activates a sugar phosphatase, which promotes dephosphorylation
513 and efflux of phosphosugars. At high levels, SgrS regulates other less essential targets
514 to switch the cellular metabolism and to use other available carbon sources. **Our study**
515 **suggests** that *S. aureus* RsaG inactivates the lactate fermentation pathway by
516 activating Rex synthesis and by repressing CcpA synthesis using different
517 mechanisms of regulation (Figure 9).

518

519 **The dual ribonuclease J1/J2 generates the 3'UTR-derived RsaG sRNA.**

520 In Gram-negative bacteria, 3'UTRs are reservoirs of sRNAs acting in trans after RNase
521 E cleavage (Kim *et al.*, 2014; Eisenhardt *et al.*, 2018; Wang *et al.*, 2020). In *S. aureus*,
522 RsaC accumulates in response to Mn starvation and is processed by RNase III from
523 the polycistronic mRNA encoding the MntABC transporter. Here, we describe the first
524 example of an sRNA for which RNases J1/J2 are required for its processing from the
525 *uhpT* mRNA, while the mRNA encoding *uhpT* is rapidly degraded. Hence RNases
526 J1/J2 are not only essential for stress responses by controlling mRNA degradation but
527 they also contribute to generate sRNA from mRNAs. Very recently, a rather similar
528 degradation mechanism was described in the maturation of the T-box riboswitch in the
529 5' UTR of the *metICFE-mdh* operon (Wencker *et al.*, 2021). Indeed, in absence of
530 methionine and after cleavage of the met leader by RNase III, the RNases J1/J2
531 mediate degradation of the mRNA from the 5' end generating more stable transcripts
532 towards the 3' end. We postulate that specific structural features of the RNAs may

533 protect them from degradation. Most likely, the 5' hairpin structure of RsaG might
534 certainly block the action of the exoribonuclease activity (Figure 3D).

535 Intriguingly, RsaG is the **fifth** example of a 3'UTR-derived sRNA issued from a
536 mRNA encoding metabolically active transporters. In *S. aureus* RsaC is processed
537 from the staphylococcal MntABC transporter of manganese and represses SodA
538 activity, which needs Mn as cofactor (Lalaouna et al., 2019). In *E. coli* NarS is
539 generated from the NarK transporter of nitrate in anaerobiosis. Nitrate is then reduced
540 in nitrite by NarG, and to limit nitrite toxicity, NarS is transcribed together with *narK* to
541 reduce the expression of *nirC* encoding the nitrite transporter (Wang et al., 2020). **The**
542 **sRNA MalH derived from the processing of the 3'UTR of the polycistron *malEFG***
543 **encoding the maltose ABC-transporter stimulates the use of alternative carbon**
544 **sources in presence of maltose (Bar et al, 2021; Iosub et al, 2021).** Finally, in *Vibrio*
545 *cholerae* OppZ is issued from the OppA oligopeptide transporter, and binds to the
546 second gene of the *oppABCDF* operon mediating repression of OppB synthesis
547 (Lalaouna et al., 2019; Wang et al., 2020; Hoyos et al., 2020). Overall, sRNAs
548 generated from mRNAs contribute to the same metabolic pathway or help bacteria to
549 choose the most appropriate way to adapt or protect the bacteria to different metabolic
550 niches in response to the effector entry. It is tempting to propose that such dual
551 partners (transporter and sRNA) are more widespread than expected. While RsaG is
552 cotranscribed with the *uhpT* transcript, we were unable to show its direct role in G6P
553 catabolism. In other pathogenic bacteria such as *Shigella flexneri* and *Listeria*
554 *monocytogenes*, their corresponding *uhpT* mRNAs do not possess large 3'UTRs but
555 are highly overexpressed during internalization (Chico-Calero et al., 2002; Runyen-
556 Janecky and Payne, 2002). In *Listeria*, *uhpT* is regulated by the major regulator PrfA,
557 and the deletion mutant of *uhpT* did not proliferate intracellularly or survive in a murine
558 model of infection (Chico-Calero et al., 2002). Although the role of UhpT in
559 staphylococcal virulence requires further investigation, we hypothesized that the
560 accumulation of RsaG would regulate additional metabolic functions when *S. aureus*
561 is internalized into the microaerophilic cytoplasm of host cells or in presence of mucus-
562 secreting cells.

563

564 **RsaG expands the regulon of HptRS.**

565 In order to scrutinize the functional impact of RsaG, we performed MAPS in presence
566 of G6P to mimic inducing conditions. **Gel retardation assays showed *in vitro* that RsaG**

567 recognized a high number of RNAs with various binding affinities, which illustrate a
568 possible hierarchical regulation. However, binding affinities *in vivo* might be different
569 as the sRNA is expected to bind the mRNA co-transcriptionally and trans-acting factors
570 might also modulate the mRNA structure and facilitate the pairings (Reyer et al., 2021).
571 Among the target RNAs, none of them are directly linked to the G6P catabolism *per se*
572 but some of them are involved in carbohydrate-dependent metabolic pathways (*ccpA*,
573 *ldh1*) and to redox homeostasis (*rex*). It is known that in the presence of glucose, CcpA
574 repressed *uhpT* and the effect was more pronounced in the late exponential phase of
575 growth (Reed et al., 2018). In contrast, HptRS activated *uhpT* in presence of G6P (Park
576 et al., 2015). Comprehensively CcpA and HptRS share the same regulon but function
577 in an opposite manner to respond to changes in the availability of glucose or G6P
578 (Reed et al., 2018). Hence, *uhpT* activation by HptRS would be required to alleviate
579 the CcpA inhibition of *uhpT* in presence of G6P. Remarkably, we also identified *ptsH*
580 as a potential target of RsaG. This mRNA encodes HPr, an activator of CcpA, which
581 is dependent on G6P for its phosphorylation and activation. Through the regulation of
582 HPr and CcpA, RsaG would add another level of regulation to favour G6P uptake in
583 detrimental to glycolysis and carbon catabolite repression (Figure 9). Such a regulation
584 is expected to be transient as CcpA is required for glycolysis, which might explain why
585 we could not visualize a significant impact of RsaG on CcpA levels. Interestingly,
586 MAPS analysis also revealed that several CcpA-regulated genes, such as *ldh1*, *ald1*,
587 *adh*, *treB*, *buA1B* (*alsS/D*), and *hemC-hemX* might also be under RsaG control (Table
588 S1 and Seidl et al., 2009). While CcpA inhibits transcription of *ald1*, *adh*, *budA1B*, it
589 activates Ldh1 activity. It is tempting to propose that RsaG accumulation reroutes the
590 bacterial metabolism leading to the inhibition of lactate fermentation while amino acid
591 catabolism, acetoine synthesis, and alcohol fermentation would be activated (Figure
592 9).

593 Another important target of RsaG is *rex* mRNA, which senses the bacterial
594 redox through changes in the NADH-NAD⁺ ratio of the bacteria. This ratio can be
595 changed dramatically under different metabolic status with or without a change in
596 oxygen viability. For instance, NADH increases during glycolysis, during the activation
597 of the TCA cycle, and under anaerobic conditions. It is known that Rex-NADH
598 dissociates from its promoter allowing transcription of numerous genes involved in
599 electron transport, in nitrogen and anaerobic metabolism (*nirC*, *narG*, *arcA*, *pflB*, *adhE*,
600 *adh*, *ldh1*, *ald1*) (Pagels et al., 2010). Interestingly among the potential direct targets,

601 RsaG can also interact with *nirC*, *arcA*, *adh* mRNAs (Table S1) and in addition induces
602 rapid degradation of *ldh1* mRNA (Figure 6C). Through the activation of *rex* and the
603 repression of *ldh1*, *nirC* and *adh*, RsaG would modulate the redox status.

604 Moreover, RsaG binds to several mRNAs encoding transcriptional factors of the
605 Sar family. Particularly, SarA is one of the most important transcriptional activator of
606 the quorum sensing operon *agr*, and facilitates the binding of the response regulatory
607 protein AgrA. We showed that RsaG hinders the binding of the ribosome to *sarA* mRNA.
608 Interestingly, SarA also inhibits the transcription of *sodM* which is required for the
609 oxidative stress resistance in presence of methyl viologen or diamide (Seidl *et al.*, 2009;
610 Ballal and Manna, 2009). Additionally, when staphylococcal cultures were starved in
611 Mn, the atypical sRNA RsaC blocked translation of *sodA*, a Mn-dependent superoxide
612 dismutase, while SodM was enhanced most probably because RsaC inhibited *sarA*
613 translation (Lalaouna *et al.*, 2019). Hence, RsaG might be a second sRNA, which links
614 oxidative stress to virulence, when G6P is used as the carbon source. RsaG interacted
615 also with two other mRNAs encoding SarV, an inducer of autolysis, and SarX, which
616 is involved in biofilm formation. Although the mechanism of regulation is awaiting
617 further experimental evidence, *in silico* predictions suggested that RsaG would bind
618 close to the RBS of these two mRNAs (Table S1).

619

620

621

622 **RsaG has two functional domains differently modulated by another sRNA.**

623 Our data showed that RsaG contained two functional domains, including the 5' hairpin
624 loop and the interhelical unpaired region, both containing C-rich motif. However, we
625 had difficulties to design mutations in RsaG to better assign the basepairing schemes
626 with its various targets indicating that alternative pairings were taking place. A similar
627 observation was done in *Enterobacteriaceae* for the regulation of the *cycA* mRNA,
628 which is repressed by the sRNA GcvB. At least five binding sites were predicted and
629 none of them were validated *in vivo* suggesting redundancy between multiple regions
630 of GcvB to *cycA* (Lalaouna *et al.*, 2018b). Nevertheless, the first C-rich motif was
631 demonstrated as the main site for RsaI, a sRNA which is repressed by CcpA, and
632 which is activated when glucose is consumed (Bronesky *et al.*, 2019). RsaI favoured
633 glucose fermentation in lactate by indirectly inducing *ldh1* mRNA (Bronesky *et al.*,

634 2019). Because RsaI competes with *rex* mRNA for RsaG binding (Figure 7), *rex*
635 activation would thus be impaired leading to Ldh1 activation.

636 The second C-rich motif located in the interhelical region of RsaG contains the
637 binding sites for *sarA*, *tcaR*, *nirC*, *ldh1* and two common targets of RsaI, *treB* and *fn3K*.
638 *In vivo*, *fn3K* and *ldh1* mRNAs are degraded faster when RsaG is present at high levels.
639 The fructosamine 3-kinase (*fn3k*) plays a role in protein deglycation by phosphorylating
640 preferentially proteins bound-ribulosamines and erythrulosamines but not
641 fructosamines, in bacteria. It has been suggested that bacterial fructosamine kinases
642 inactivate exogenous toxic compounds like the aminoglycosides or macrolides, but the
643 internal substrate remains unknown (Gemayel *et al.*, 2007). The interaction of RsaG
644 or RsaI to *fn3K* mRNA leads respectively to mRNA degradation when G6P is present
645 or inhibition of translation in absence of glucose. At least *in silico*, the binding site of
646 RsaI and RsaG on *fn3K* mRNAs are different suggesting that RsaI would modulate
647 only part of the functions of RsaG. Similarly, *in vitro*, RsaI does not affect the binding
648 of *tdcB*, another common target, which interacts with the apical loop of RsaG or of
649 *sarA*, which does not interact with RsaI (Figure 7).

650 Our data suggested that the interaction between RsaG and RsaI might
651 contribute to hierarchical and temporal regulation in order to promote efficient and
652 dynamic cell responses to G6P entry. Quantitative analysis will be certainly required
653 to better decipher the roles of RsaG and the regulatory priority for its targets as it was
654 demonstrated for SgrS during glucose-phosphate stress (Bobrovskyy *et al.*, 2019).

655 **RsaG study led to evolutionary considerations.**

657 A recent genome-wide comparative analysis of orthologous mRNAs from
658 *Staphylococcus* highlighted a high diversity in the length and sequence of the 3'UTRs
659 (Menendez-Gil *et al.*, 2020). Using chimeric constructs carrying various orthologous
660 3'UTRs, variation in protein synthesis of the corresponding gene was observed
661 suggesting that these regions contribute to differentially regulate gene expression by
662 a species-specific mechanism (Menendez-Gil *et al.*, 2020). This hypothesis is also in
663 agreement with the role of 3'UTRs in eukaryotes, which contributed to the divergence
664 of species by evolving regulatory elements (Cheng *et al.*, 2009). It is intriguing that
665 RsaG is conserved only in closely related species as *S. argenteus* and *S. schweitzeri*,
666 while *uhpT* is universal. Interestingly, in the ape pathogen *S. simiae*, we detected a
667 long (726 nucleotides) and stable RNA probably processed from the 3'UTR of *uhpT*

668 mRNA. The sequence is not homologous to RsaG and RNA accumulation does not
669 depend on presence of G6P. As UhpT mediates the exchange of external hexose-6-
670 phosphate, it remains to be explored what is the preferred carbon source that is sensed
671 by UhpT in *S. simiae*. However, the 3'UTR contains several repeats with C-rich motifs,
672 and only interaction sites were predicted between a C-rich motif and a region upstream
673 of the SD of *ccpA*. We suggest that the acquisition of RsaG has evolved together with
674 the acquisition of *Staphylococcus* pathogenesis in order to facilitate a better
675 adaptation/protection of the bacteria during infection. We also do not exclude that in
676 the distant staphylococcal species, other sRNAs encoded from different locus of the
677 genome might play similar functions as RsaG.

678 Another level of complexity was added by a recent re-analysis of ribosome
679 profiling data identifies several sRNAs with potential capacity to encode peptides
680 (Sorensen et al., 2020). Among these candidates, RsaG was suspected to contain an
681 open reading frame leading to a 25 amino acid long peptide although experimental
682 validation is still missing. If RsaG is endowed with coding properties, experiments will
683 be necessary to decipher the function of the peptide, to analyse whether a temporal
684 factor regulates the dual functions of RsaG, and whether the translation event might
685 interfere with its regulatory properties. It will be essential to demonstrate whether the
686 two functions act in the same pathway as SgrS in enterobacteria, which protects the
687 cell against glucose-phosphate stress, or whether the two functions act in independent
688 pathway as *S. aureus* RNAIII (Raina et al., 2018).

689 In conclusion, acquisition of glucose transporters such as GlcC transporters was
690 described as an adaptative advantage for *S. aureus* to survive within host tissue when
691 O₂ is rare (Vitko et al., 2016). By analogy, we could postulate that *uhpT* transporter
692 has evolved a functional 3'UTR (RsaG) because it is necessary to uptake G6P, and
693 concomitantly to adapt metabolism and redox homeostasis when *S. aureus* is
694 internalized or in presence of mucus-producing cells.

695

696 **EXPERIMENTAL PROCEDURE**

697

698 **Strains and plasmids**

699 All strains and plasmids, constructed and used in this study, are described in Table
700 S2. The oligonucleotides sequences are given in Table S3. *E. coli* strain DH5 α was
701 used for cloning purposes. *E. coli* strain DC10B, a DNA cytosine methyltransferase

702 negative mutant and *S. aureus* RN4220 were used for plasmid amplification before *S.*
703 *aureus* HG001 transformation. Transformation of *E. coli* was performed by heat shock
704 and *S. aureus* by electroporation (Bio-Rad Gene Pulser). The plasmids were extracted
705 from *E. coli* or *S. aureus* with the Nucleospin Plasmid kit (Macherey-Nagel) adding a
706 mechanical breakage of staphylococcal cells with FastPrep in P1 buffer. **Deletions** of
707 *rsaG* and *uhpT* promoter comprised respectively removal of nucleotides 201739 to
708 201936 and nucleotides 200154 to 200282 (Caldelari *et al.*, 2017) and were
709 constructed by homologous recombination using the thermosensitive vector pMAD
710 (Arnaud *et al.*, 2004). Chromosomal regions upstream or downstream of *rsaG* or *uhpT*
711 promoter were amplified by PCR (see table S3 for primers) and cloned into pMAD. The
712 resulting plasmid was electroporated first into RN4220 recipient strain and then into
713 HG001. Transformants were grown at non-permissive temperature (44°C), followed by
714 several subcultures at 28°C and 37°C to favour double crossing over as previously
715 described (Arnaud *et al.*, 2004). To generate the plasmid expressing *rsaG* for
716 complementation, the entire gene (194 bp) was PCR amplified with the following
717 oligonucleotides: RsaG *PstI* for and RsaG *BamHI* rev (Table S3), digested by *PstI* and
718 *BamHI* and ligated into pCN51::P3 digested with the same enzymes (Tomasini *et al.*,
719 2017) to obtain pCN51::P3::*rsaG*. The MS2 tag was fused to the 5' end of *rsaG* using
720 oligonucleotides *PstI*-MS2-RsaG for and RsaG-*BamHI* rev cloned into *PstI*/*BamHI*-
721 digested pCN51::P3. The pUC-T7::*rsaG* mut1, mut2 and mut1/2 vectors were obtained
722 by QuickChange XL Site-directed mutagenesis (Stratagene) from pUC-T7::*rsaG*.

723 For transcriptional fusions, different length fragments of the *uhpT* upstream
724 region (i.e. 1585, 1456, 500, 250, 100 bp before RsaG transcription start site) (see
725 Table S3 for primers sequences et description) were cloned into *SphI*-*BamHI*-digested
726 pEW-GFP plasmid containing the 5'UTR_{hly} from *Listeria monocytogenes*
727 (Menendez-Gil *et al.*, 2020). Translational fusion to *lacZ* was constructed in
728 pLUG220::*rpoB*::*lacZ* (Romilly *et al.*, 2014). First, a 309 bp fragment containing the
729 5'UTR region of *rex* mRNA and 69 codons (-103/+207 bp) was amplified with primers
730 *rex* for *BamHI* and *rex* rev *BamHI* and cloned into *BamHI*-digested
731 pLUG220::*rpoB*::*lacZ* to generate pLUG220::*rpoB*::*rex*::*lacZ*. Then an amplicon
732 containing *rsaG* under the *blaZ* promoter was produced by two distinct PCR. The
733 pCN40 plasmid was used as template to amplify *blaZ* promoter with primers *PstI*-
734 pBlaZ-pES for/RsaG-pBlaZ-pES3 rev and HG001 genomic DNA to amplify *rsaG* with
735 primers RsaG for/*PstI*-RsaG rev. The two PCR products served as template for a PCR

736 with oligonucleotides *PstI*-pBlaZ-pES for/ *PstI*-RsaG rev and ligated into the *PstI*-
737 digested pLUG220::*rpoB*::*rex*::*lacZ*.

738

739 **Growth conditions**

740 *E. coli* strains were grown in Lysogeny-Broth (LB, Roth) medium supplemented with
741 ampicillin (100 µg/mL) or kanamycin (30 µg/mL) when necessary. *S. aureus* strains
742 were cultivated in Brain-Heart infusion (BHI, Sigma) or Muller Hinton Broth (MHB,
743 Sigma) media containing 10 µg/mL of erythromycin when needed. To induce RsaG,
744 MHB or BHI were complemented with 0.5% of glucose-6-phosphate (G6P) (Sigma).

745

746 **Northern blot**

747 Purification of total RNA extracts was performed strictly following the procedure
748 described for the FastRNA pro blue kit (MP Biomedicals) with the Fastprep apparatus
749 (MP Biomedicals). Electrophoresis of 10 µg of total RNA was run in a 1% TBE-agarose
750 gel, containing 25 mM guanidium thiocyanate (Sigma). After migration, RNAs were
751 transferred on Hybond N+ nitrocellulose membrane (GE Healthcare Life Sciences) by
752 vacuum with the vacuum-blot system (Whayman biometra) or by capillarity and fixed
753 by UV-crosslinking (Stratalinker 1800 Stratagene). RNA detection was performed by
754 hybridization with specific digoxigenin (DIG)-labeled probes complementary to each
755 targeted RNA as described previously (Tomasini *et al.*, 2017).

756

757 **Western blot and microscopy**

758 Total proteins were extracted from cultures grown for 4 h in BHI before harvesting by
759 centrifugation. Bacterial pellets were resuspended in 1X PBS and lysed using the
760 Fastprep (MP Biomedicals). Quantification of proteins was performed with Bradford
761 reagent following the manufacture protocol (BioRad) and BSA as the standard. Equal
762 amounts (0.5 µg) of total proteins were migrated on 12% polyacrylamide-SDS- gels
763 and transferred onto PVDF membranes with a Trans-blot Turbo Transfer system
764 (BioRad). Blots were incubated with anti-GFP at the final dilution 1:5000 followed by
765 an incubation with a goat anti-mouse peroxidase (HRP) (Biorad) at the final dilution
766 1:5000. Gels were stained by Coomassie blue as loading controls of samples.

767 For fluorescent microscopy, 10 µl of the same cultures were spread between
768 slide and coverslip and observed with Epifluorescence microscope TiE, Nikon
769 (excitation source: LED Spectra X, Lumencor, camera: Orca-Flash IV, objectif: Plan

770 Apo x100 oil, numerical aperture: 1;45) under excitation at 475 nm and emission at
771 514 +/- 24nm.

772

773 **MAPS analyses**

774 Crude bacterial extracts were prepared in duplicates from cultures of Δ rsaG strain
775 expressing MS2-RsaG or from WT strain expressing MS2 grown for 5 h in BHI and
776 then 0.5% G6P was added for another hour of incubation before harvesting and lysis
777 as previously described (Lalaouna *et al.*, 2018a). After MS2-affinity chromatography,
778 RNA was purified from the elution fraction and used either for Northern Blot or DNase I
779 treated prior to RNA-seq analysis as described (Lalaouna *et al.*, 2018a). The
780 enrichment values were calculated by DEseq2 (P -adj < 0.05; fold change > 2) as
781 previously published (Tomasini *et al.*, 2017).

782

783 **Preparation of RNAs for *in vitro* experiments**

784 Transcription of RsaG or RsaI was achieved with linearized pUC18 vectors
785 (Geissmann *et al.*, 2009; Bronesky *et al.*, 2019). PCR fragments containing RsaG mut1,
786 RsaG mut2 and RsaG mut1/2, the 5'UTR of selected mRNAs or **the synthetic gene**
787 **encoding the rex R2 mRNA (Integrated DNA Technologies)** downstream the sequence
788 of the T7 promoter were used as templates for *in vitro* transcription using T7 RNA
789 polymerase (see Table S3 for oligonucleotides and sizes of DNA fragments). RNAs
790 were purified from 6% or 8% polyacrylamide-8 M urea gel, eluted with 0.5 M
791 ammonium acetate pH 6.5, 1 mM EDTA and 0.1 % SDS and finally precipitated in cold
792 absolute ethanol. Dephosphorylated RNAs were labeled with T4 polynucleotide kinase
793 (Fermentas) and [γ ³²P] ATP.

794

795 **Gel retardation assay**

796 The 5' end radioabeled RsaG, the mutants RsaG mut1, RsaG mut2, RsaG mut1/2,
797 **RsaG mut3, and RsaG mut4** (10'000 cps/sample, < 1 pM) and cold mRNAs were
798 renatured separately by incubation at 90°C for 1 min in 100 mM Tris-HCl pH 7,5, 300
799 mM KCl, 200 mM NH₄Cl, cooled down 1 min on ice, and incubated at 20°C 10 min in
800 presence of 10 mM MgCl₂. Complexes were formed at 37°C for 15 min, then 10 μ l of
801 glycerol blue was added and the samples loaded on a native 6% polyacrylamide gel
802 containing 10 mM MgCl₂ (4-6 h, 300 V, 4°C).

803

804 **Toe-printing assays**

805 The preparation of 30S subunits of *S. aureus* was described elsewhere (Khusainov *et*
806 *al.*, 2017), likewise the extension inhibition conditions (Fechter *et al.*, 2009). Increasing
807 concentrations of RsaG were used to monitor its effect on the simplified translational
808 initiation complex formed with *S. aureus* 30S ribosomal subunits, initiator tRNA^{fMet} and
809 mRNAs.

810

811 **Primer extension assays**

812 In order to determine the transcriptional start site of RsaG from *S. simiae*, 15 µg of total
813 RNA from a bacterial culture grown in presence or absence of G6P was reversed
814 transcribed with the AMV reverse transcriptase (NEB) and the 5'-radiolabeled
815 oligonucleotide RsaG-like rev. The reaction was performed and analysed as previously
816 described (Lalaouna *et al.*, 2019). The sequencing ladder was obtained with a PCR
817 product using oligonucleotides RsaG-like for/RsaG-like rev.

818

819 **Monitoring of the 5' extremity of RsaG**

820 TerminatorTM 5'-Phosphate-dependent exonuclease Terminator (Epicentre) enzyme
821 degrades secondary transcripts carrying a mono-phosphate 5' extremity but has no
822 effect on primary transcript displaying a tri-phosphate 5' extremity and also on highly
823 structured transcript as 5S rRNA. Total RNA (10 µg) was extracted from HG001 strain
824 grown for 4 h culture in BHI with or without G6P 0.5 % and incubated for 1 h at 30°C
825 with Terminator Exonuclease (1U) and Terminator 1X Reaction buffer A. RNAs were
826 then purified with phenol-chloroform alcohol isoamyl extraction and ethanol
827 precipitation. Northern blot experiment was performed on 1% agarose gel containing
828 25 mM guanidium thiocyanate.

829

830 **Co-culture experiments**

831 Human colon epithelial HT29 and HT29MTX, human tumorigenic lung epithelial A549
832 and human tumorigenic liver HU-H7 cell lines were maintained in Dulbecco's Modified
833 Eagle's Medium (DMEM) (Thermofisher) medium with 10% FCS and 1% penicillin-
834 streptomycin (Gibco) at 37°C under 5% CO₂ atmosphere. At 4 days or 14 days (HT29
835 and HT29MTX cells), cells are plated in 100 X 20 mm Petri dishes at 0.75x10⁶ cells for
836 HU-H7, 10⁶ cells for A549 and 1.5x10⁶ cells for HT-29 and HT-29MTX. Then 10 ml of
837 HG001 or HG001 $\Delta hptRS$ grown for 4 h in MHB, when RsaG is poorly expressed (ca.

838 OD_{600nm} = 1) are added to human cells for 1 h at 37°C. As controls, fresh 10 ml MHB
839 was added to cells and 10 ml of HG001 bacterial culture was incubated with or without
840 0.5% G6P. Then supernatants of human cells were carefully collected and centrifuged.
841 Bacterial pellets were used to extract total RNA, which is analysed by Northern blot
842 and supernatants were examined for the presence of mucus by dot blot experiments.
843

844 **Dot Blot assay**

845 1 µl (or 4 µl supernatant of infected HT-29 cells) of co-cultures supernatants or non-
846 infected supernatants was drop on a PVDF membrane activated with ethanol 95% and
847 equilibrated in TBS 1X Tween 0.1%. The membranes were incubated with a rabbit
848 anti-Muc2 or a mouse anti-Muc5AC at the final dilution of 1:1000 followed by
849 respectively a goat anti-rabbit and a goat anti-mouse at the final dilution of 1:10000.
850

851 **Quantification of intracellular expression**

852 The human myoblasts CTi400 were cultured in KMEM medium (1v M199, 4v DMEM),
853 20% fetal bovine serum (v/v), 25 µg/ml Fetuin, 0.5 ng/ml bFGF, 5 ng/ml EGF, 5 µg/ml
854 Insulin, 0.2 mg/ml dexamethasone at 37°C under 5% CO₂ atmosphere. The murine
855 macrophages RAW 264.7 were cultured in DMEM (Thermofisher) supplemented with
856 10% FBS at 37°C under 5% CO₂ atmosphere.

857 The intracellular infection of cells was performed using gentamycin protection
858 assay as previously described (Trouillet *et al.*, 2011) with modifications. Cells were
859 seeded at 80,000 cells per well in 24-well tissue culture plates. After 24 h, cells were
860 washed twice with 1 mL of PBS and infected at a multiplicity of infection (MOI) of 10:1
861 with bacterial culture (9 h of growth) diluted in cell medium antibiotic free. The MOI was
862 confirmed by CFU counting upon agar plate inoculation. After 2 h of infection at 37°C,
863 cells were washed twice with 1 mL of PBS and incubated for 1 h in medium containing
864 200 µg/mL gentamicin and 10 µg/mL lysostaphin to kill extracellular bacteria. After the
865 antibiotic treatment, 3 wells were pooled, cells and bacteria were harvested by trypsin
866 detachment and centrifugation. As controls, bacteria were incubated for 1 h in KMEM
867 medium or DMEM under the same conditions as above.

868 To quantify RsaG, pellets were treated with 20 µg lysostaphin and RNA isolation
869 was performed using the RNeasy Plus mini kit (QIAGEN) according to the
870 manufacturer's instructions. The RNA was quantified using a NanoDrop
871 spectrophotometer, and 150 ng of total RNA was reverse transcribed into cDNA using

872 Reverse Transcriptase System (Promega). 1 μ L of 1/5 diluted cDNA was used as
873 template for the real-time PCR amplification using PowerUp SYBR® Green Master Mix
874 and a StepOne Plus system (Applied Biosystem) with specific primers shown in Table
875 S3. Relative RsaG amount analysis was performed by using Δ Ct methods using *gyrB*
876 gene as an internal standard and confirmed by *hu* and 16S gene (see Table S3 for
877 oligonucleotides).

878

879 **DATA AVAILABILITY STATEMENT**

880 MAPS data are openly available in the public repository GEO under accession [GSE176028](#).

881

882 **SUPPLEMENTARY DATA**

883 Supplementary data are available.

884

885

886

887 **ACKNOWLEDGMENTS**

888 The cell lines (HT-29, HT-29 MTX), the antibodies (anti-MUC-2 and anti-MUC-5CA)
889 were kindly supplied by Dr. Benoît Marteyn (IBMC, Strasbourg), the A549 cell line by
890 Dr. Alain Lescure (IBMC, Strasbourg), and the Hu-H7 cell line by Dr. Catherine
891 Schuster (Institut de virologie, Strasbourg). We are thankful to Delphine Bronesky and
892 David Lalaouna for helpful discussions, and Anne-Catherine Helfer who has performed
893 footprinting experiments.

894

895 **FUNDING**

896 This work was supported by the Centre National de la Recherche Scientifique (CNRS),
897 by the French National Research Agency ANR (ANR-18-CE12-0025-04 CoNoCo to
898 [P.R.]). This work of the Interdisciplinary Thematic Institute IMCBio, as part of the ITI
899 2021-2028 program of the University of Strasbourg, CNRS and Inserm, was supported
900 by IdEx Unistra (ANR-10-IDEX-0002) and by SFRI-STRAT'US (ANR 20-SFRI-0012),
901 and EUR IMCBio (IMCBio ANR-17-EURE-0023) under the framework of the French
902 Investments for the Future Program. ED and LB were supported by the "Fondation
903 pour la Recherche Médicale" (FDT201904007957 and ECO202006011534).

904

905 **REFERENCES**

906

907 Afgan, E., Baker, D., Beek, M. van den, Blankenberg, D., Bouvier, D., Čech, M., *et al.*
908 (2016) The Galaxy platform for accessible, reproducible and collaborative biomedical
909 analyses: 2016 update. *Nucleic Acids Research* **44**: gkw343.

910

911 Ando, M., Manabe, Y.C., Converse, P.J., Miyazaki, E., Harrison, R., Murphy, J.R., and
912 Bishai, W.R. (2003) Characterization of the Role of the Divalent Metal Ion-Dependent
913 Transcriptional Repressor MntR in the Virulence of *Staphylococcus aureus*. *IAI* **71**:
914 2584–2590.

915

916 Arnaud, M., Chastanet, A., and Débarbouillé, M. (2004) New Vector for Efficient Allelic
917 Replacement in Naturally Nontransformable, Low-GC-Content, Gram-Positive
918 Bacteria. *Appl Environ Microbiol* **70**: 6887–6891.

919

920 Augagneur, Y., King, A.N., Germain-Amiot, N., Sassi, M., Fitzgerald, J.W., Sahukhal,
921 G.S., *et al.* (2020) Analysis of the CodY RNome reveals RsaD as a stress-responsive
922 riboregulator of overflow metabolism in *Staphylococcus aureus*. *Mol Microbiol* **113**:
923 309–325.

924

925 Ballal, A., and Manna, A.C. (2009) Regulation of Superoxide Dismutase (sod) Genes
926 by SarA in *Staphylococcus aureus*. *JB* **191**: 3301–3310.

927

928 Bar, A., Argaman, L., Altuvia, Y., and Margalit, H. (2021). Prediction of novel bacterial small
929 RNAs from RIL-Seq RNA-RNA interaction data. *Front in Microbiol* **12**: 635070.

930

931 Behrens, I., Stenberg, P., Artursson, P., and Kissel, T. (2001) Transport of lipophilic
932 drug molecules in a new mucus-secreting cell culture model based on HT29-MTX cells.
933 *Pharmaceutical Research* **18**: 1138–1145.

934

935 Bobrovskyy, M., and Vanderpool, C.K. (2013) Regulation of Bacterial Metabolism by
936 Small RNAs Using Diverse Mechanisms. *Annu Rev Genet* **47**: 209–232.

937

938 Bobrovskyy, M., Azam M.S., Frandsen, J.K., Zhang, J., Poddar, A., Ma, X., Henkin,
939 T.M., Ha, T., and Vanderpool, C. K. (2019) Determinants of target prioritization and
940 regulatory hierarchy for the bacterial small RNA SgrS. *Mol Microbiol* **112**(4): 1199-1218.

941

942 Brandenberger, M., Tschierske, M., Giachino, P., Wada, A., and Berger-Bächi, B.
943 (2000) Inactivation of a novel three-cistronic operon *tcaR-tcaA-tcaB* increases
944 teicoplanin resistance in *Staphylococcus aureus*. *Biochimica et Biophysica Acta (BBA)*
945 - *General Subjects* **1523**: 135–139.

946

947 Bronesky, D., Desgranges, E., Corvaglia, A., François, P., Caballero, C.J., Prado, L.,
948 *et al.* (2019) A multifaceted small RNA modulates gene expression upon glucose
949 limitation in *Staphylococcus aureus*. *The EMBO Journal* e99363.

950

951 Brosse, A., and Guillier, M. (2018) Bacterial Small RNAs in Mixed Regulatory Networks.
952 *Microbiol Spectr* **6**.

953

954 Caldelari, I., Chane-Woon-Ming, B., Noirot, C., Moreau, K., Romby, P., Gaspin, C.,
955 and Marzi, S. (2017) Complete Genome Sequence and Annotation of the

- 956 *Staphylococcus aureus* Strain HG001. *Genome Announc* **5**: e00783-17,
957 /ga/5/32/e00783-17.atom.
- 958
- 959 Chatterjee, S.S., Joo, H.-S., Duong, A.C., Dieringer, T.D., Tan, V.Y., Song, Y., *et al.*
960 (2013) Essential *Staphylococcus aureus* toxin export system. *Nat Med* **19**: 364–367.
- 961
- 962 Cheng, C., Bhardwaj, N., and Gerstein, M. (2009) The relationship between the
963 evolution of microRNA targets and the length of their UTRs. *BMC Genomics* **10**: 431.
- 964
- 965 Cheung, A.L., Nishina, K.A., Trottonda, M.P., and Tamber, S. (2008) The SarA protein
966 family of *Staphylococcus aureus*. *The international journal of biochemistry & cell*
967 *biology* **40**: 355–361.
- 968
- 969 Chico-Calero, I., Suarez, M., Gonzalez-Zorn, B., Scotti, M., Slaghuis, J., Goebel, W.,
970 *et al.* (2002) Hpt, a bacterial homolog of the microsomal glucose- 6-phosphate
971 translocase, mediates rapid intracellular proliferation in *Listeria*. *Proceedings of the*
972 *National Academy of Sciences* **99**: 431–436.
- 973
- 974 Christmas, B.A.F., Rolfe, M.D., Rose, M., and Green, J. (2019) *Staphylococcus aureus*
975 adaptation to aerobic low-redox-potential environments: implications for an
976 intracellular lifestyle. *Microbiology* **165**: 779–791.
- 977
- 978 Crooke, A.K., Fuller, J.R., Obrist, M.W., Tomkovich, S.E., Vitko, N.P., and Richardson,
979 A.R. (2013) CcpA-Independent Glucose Regulation of Lactate Dehydrogenase 1 in
980 *Staphylococcus aureus*. *PLoS ONE* **8**: e54293.
- 981
- 982 Desgranges, E., Marzi, S., Moreau, K., Romby, P., and Caldelari, I. (2019) Noncoding
983 RNA. *Microbiology Spectrum* **7**
984 [http://www.asmscience.org/content/journal/microbiolspec/10.1128/
985 microbiolspec.GPP3-0038-2018](http://www.asmscience.org/content/journal/microbiolspec/10.1128/microbiolspec.GPP3-0038-2018). Accessed June 23, 2020.
- 986
- 987 Deutscher, J., Küster, E., Bergstedt, U., Charrier, V., and Hillen, W. (1995) Protein kinase-
988 dependent HPr/CcpA interaction links glycolytic activity to carbon catabolite repression in
989 Gram-positive bacteria. *Mol. Microbiol.* **15**:1049–1053.
- 990
- 991 Eisenhardt, K.M.H., Reuscher, C.M., and Klug, G. (2018) PcrX, an sRNA derived from
992 the 3'- UTR of the *Rhodobacter sphaeroides puf* operon modulates expression of *puf*
993 genes encoding proteins of the bacterial photosynthetic apparatus. *Molecular*
994 *Microbiology* **110**: 325–334.
- 995
- 996 Fechter, P., Chevalier, C., Yusupova, G., Yusupov, M., Romby, P., and Marzi, S. (2009)
997 Ribosomal initiation complexes probed by toeprinting and effect of trans-acting
998 translational regulators in bacteria. *Methods Mol Biol* **540**: 247–263.
- 999
- 1000 Garzoni, C., Francois, P., Huyghe, A., Couzinet, S., Tapparel, C., Charbonnier, Y., *et*
1001 *al.* (2007) A global view of *Staphylococcus aureus* whole genome expression upon
1002 internalization in human epithelial cells. *BMC Genomics* **8**: 171.
- 1003
- 1004 Geissmann, T., Chevalier, C., Cros, M.-J., Boisset, S., Fechter, P., Noirot, C., *et al.*
1005 (2009) A search for small noncoding RNAs in *Staphylococcus aureus* reveals a

- 1006 conserved sequence motif for regulation. *Nucl Acids Res* **37**: 7239–7257.
1007
- 1008 Gemayel, R., Fortpied, J., Rzem, R., Vertommen, D., Veiga-da-Cunha, M., and Van
1009 Schaffingen, E. (2007) Many fructosamine 3-kinase homologues in bacteria are
1010 ribulosamine/erythrulosamine 3-kinases potentially involved in protein deglycation:
1011 Bacterial fructosamine 3-kinase homologues. *FEBS Journal* **274**: 4360–4374.
1012
- 1013 Guerrier-Takada, C., and Altman, S. (1984) Catalytic activity of an RNA molecule
1014 prepared by transcription in vitro. *Science* **223**: 285–286.
1015
- 1016 Hamza, T., and Li, B. (2014) Differential responses of osteoblasts and macrophages
1017 upon *Staphylococcus aureus* infection. *BMC Microbiol* **14**: 207.
1018
- 1019 Hoyos, M., Huber, M., Förstner, K.U., and Papenfort, K. (2020) Gene autoregulation
1020 by 3' UTR-derived bacterial small RNAs. *eLife* **9**: e58836.
1021
- 1022 Iosub, I.A., Marchioretto, M., van Nues, R.W., McKellaar, S., Viero, G., and Granneman, S.
1023 (2021) The mRNA derived MalH sRNA contributes to alternative carbon source utilization by
1024 tuning maltoporin expression in *E. coli*. *RNA Biology* **18**:6, 914-931.
1025
- 1026 Jefferson, K.K., Pier, D.B., Goldmann, D.A., and Pier, G.B. (2004) The Teicoplanin-
1027 Associated Locus Regulator (TcaR) and the Intercellular Adhesin Locus Regulator
1028 (IcaR) Are Transcriptional Inhibitors of the ica Locus in *Staphylococcus aureus*. *Journal*
1029 *of Bacteriology* **186**: 2449–2456.
1030
- 1031 Khusainov, I., Vicens, Q., Ayupov, R., Usachev, K., Myasnikov, A., Simonetti, A., *et al.*
1032 (2017) Structures and dynamics of hibernating ribosomes from *Staphylococcus aureus*
1033 mediated by intermolecular interactions of HPF. *EMBO J* **36**: 2073–2087.
1034
- 1035 Kim, H.M., Shin, J.-H., Cho, Y.-B., and Roe, J.-H. (2014) Inverse regulation of Fe- and
1036 Ni-containing SOD genes by a Fur family regulator Nur through small RNA processed
1037 from 3'UTR of the sodF mRNA. *Nucleic Acids Research* **42**: 2003–2014.
1038
- 1039 Kleist, S. von, Chany, E., Burtin, P., King, M., and Fogh, J. (1975) Immunohistology of
1040 the Antigenic Pattern of a Continuous Cell Line From a Human Colon Tumor. *JNCI:*
1041 *Journal of the National Cancer Institute* **55**: 555–560.
1042
- 1043 Lalaouna, D., Baude, J., Wu, Z., Tomasini, A., Chicher, J., Marzi, S., *et al.* (2019) RsaC
1044 sRNA modulates the oxidative stress response of *Staphylococcus aureus* during
1045 manganese starvation. *Nucleic Acids Research* **47**: 9871–9887.
1046
- 1047 Lalaouna, D., Desgranges, E., Caldelari, I., and Marzi, S. (2018a) MS2-Affinity
1048 Purification Coupled With RNA Sequencing Approach in the Human Pathogen
1049 *Staphylococcus aureus*. In *Methods in Enzymology*. Elsevier, pp. 393–411
1050 <https://linkinghub.elsevier.com/retrieve/pii/S007668791830301X>. Accessed January
1051 15, 2019.
1052
- 1053 Lalaouna, D., Eyraud, A., Devinck, A., Prévost, K., and Massé, E. (2018b) GcvB small
1054 RNA uses two distinct seed regions to regulate an extensive targetome. *Mol Microbiol*
1055 *mmi.14168*.

- 1056
1057 Linder, P., Lemeille, S., and Redder, P. (2014) Transcriptome-Wide Analyses of 5'-
1058 Ends in RNase J Mutants of a Gram-Positive Pathogen Reveal a Role in RNA
1059 Maturation, Regulation and Degradation. *PLoS Genet* **10**: e1004207.
1060
- 1061 Makhlin, J., Kofman, T., Borovok, I., Kohler, C., Engelmann, S., Cohen, G., and
1062 Aharonowitz, Y. (2007) *Staphylococcus aureus* ArcR Controls Expression of the
1063 Arginine Deiminase Operon. *JB* **189**: 5976–5986.
1064
- 1065 Marincola, G., Wencker, F.D.R., and Ziebuhr, W. (2019) The Many Facets of the Small
1066 Non-coding RNA RsaE (RoxS) in Metabolic Niche Adaptation of Gram-Positive
1067 Bacteria. *Journal of Molecular Biology* **431**: 4684–4698.
1068
- 1069 Menendez-Gil, P., Caballero, C.J., Catalan-Moreno, A., Irurzun, N., Barrio-Hernandez,
1070 I., Caldelari, I., and Toledo-Arana, A. (2020) Differential evolution in 3'UTRs leads to
1071 specific gene expression in *Staphylococcus*. *Nucleic Acids Research* **48**: 2544–2563.
1072
- 1073 Meydan, S., Marks, J., Klepacki, D., Sharma, V., Baranov, P.V., Firth, A.E., Margus,
1074 T., Kefi, A., Vázquez-Laslop, N., and Mankin, A.S. (2019) Retapamulin-
1075 Assisted Ribosome Profiling Reveals the Alternative Bacterial Proteome. *Mol Cell*.
1076 74(3):481-493.
1077
- 1078 Michalik, S., Depke, M., Murr, A., Gesell Salazar, M., Kusebauch, U., Sun, Z., *et al.*
1079 (2017) A global *Staphylococcus aureus* proteome resource applied to the in vivo
1080 characterization of host-pathogen interactions. *Sci Rep* **7**: 9718.
1081
- 1082 Miyakoshi, M., Chao, Y., and Vogel, J. (2015) Regulatory small RNAs from the 3'
1083 regions of bacterial mRNAs. *Current Opinion in Microbiology* **24**: 132–139.
1084
- 1085 Pagels, M., Fuchs, S., Pané-Farré, J., Kohler, C., Menschner, L., Hecker, M., *et al.*
1086 (2010) Redox sensing by a Rex-family repressor is involved in the regulation of
1087 anaerobic gene expression in *Staphylococcus aureus*: Redox sensitive gene
1088 regulation in *S. aureus*. *Molecular Microbiology* **76**: 1142–1161.
1089
- 1090 Park, J.Y., Kim, J.W., Moon, B.Y., Lee, J., Fortin, Y.J., Austin, F.W., *et al.* (2015)
1091 Characterization of a Novel Two-Component Regulatory System, HptRS, the
1092 Regulator for the Hexose Phosphate Transport System in *Staphylococcus aureus*.
1093 *Infection and Immunity* **83**: 1620–1628.
1094
- 1095 Poddar A., Azam M.S., Kayikcioglu T., Bobrovskyy M., Zhang J., Ma X., *et al.* (2021)
1096 Effects of individual base-pairs on in vivo target search and destruction kinetics of
1097 bacterial small RNA. *Nat Commun* **8**;12(1):874. doi: 10.1038/s41467-021-21144-0.
1098
- 1099 Raina, M., King, A., Bianco, C., and Vanderpool, C.K. (2018) Dual-Function RNAs. In
1100 *Regulating with RNA in Bacteria and Archaea*. Storz, G., and Papenfort, K. (eds). ASM
1101 Press, Washington, DC, USA. pp. 471–485
1102 <http://doi.wiley.com/10.1128/9781683670247.ch27>. Accessed May 18, 2021.
1103

- 1104 Reed, J.M., Olson, S., Brees, D.F., Griffin, C.E., Grove, R.A., Davis, P.J., *et al.* (2018)
1105 Coordinated regulation of transcription by CcpA and the *Staphylococcus aureus* two-
1106 component system HptRS. *PLoS ONE* **13**: e0207161.
1107
- 1108 Reyer M.A., Chennakesavalu S., Heideman E.M., Ma X., Bujnowska M., Hong L., Dinner A.R.,
1109 Vanderpool C.K., Fei J. (2021) Kinetic modeling reveals additional regulation at co-
1110 transcriptional level by post-transcriptional sRNA regulators. *Cell Rep.* 2021 Sep
1111 **28**;36(13):109764. doi: 10.1016/j.celrep.2021.109764.
1112
- 1113 Richards, G.R., Patel, M.V., Lloyd, C.R. and Vanderpool, C.K. (2013) Depletion of glycolytic
1114 intermediates plays a key role in glucose-phosphate stress in *Escherichia coli*. *J Bacteriol*
1115 **195**(21):4816-25.
1116
- 1117 Richardson, A.R. (2019) Virulence and Metabolism. *Microbiology Spectrum* **7**
1118 <http://www.asmscience.org/content/journal/microbiolspec/10.1128/microbiolspec.GP>
1119 P3-0011-2018. Accessed June 23, 2020.
1120
- 1121 Rochat, T., Bohn, C., Morvan, C., Le Lam, T.N., Razvi, F., Pain, A., *et al.* (2018) The
1122 conserved regulatory RNA RsaE down-regulates the arginine degradation pathway in
1123 *Staphylococcus aureus*. *Nucleic Acids Research* **46**: 8803–8816.
1124
- 1125 Romilly, C., Lays, C., Tomasini, A., Caldelari, I., Benito, Y., Hammann, P., *et al.* (2014)
1126 A Non-Coding RNA Promotes Bacterial Persistence and Decreases Virulence by
1127 Regulating a Regulator in *Staphylococcus aureus*. *PLoS Pathog* **10**
1128 <http://www.ncbi.nlm.nih.gov/pmc/articles/PMC3961350/>. Accessed August 1, 2016.
1129
- 1130 Runyen-Janecky, L.J., and Payne, S.M. (2002) Identification of Chromosomal *Shigella*
1131 *flexneri* Genes Induced by the Eukaryotic Intracellular Environment. *IAI* **70**: 4379–4388.
1132
- 1133 Seidl, K., Müller, S., François, P., Kriebitzsch, C., Schrenzel, J., Engelmann, S., *et al.*
1134 (2009) Effect of a glucose impulse on the CcpA regulon in *Staphylococcus aureus*.
1135 *BMC Microbiol* **9**: 95.
1136
- 1137 Sit, B., Crowley, S.M., Bhullar, K., Lai, C.C.-L., Tang, C., Hooda, Y., *et al.* (2015) Active
1138 Transport of Phosphorylated Carbohydrates Promotes Intestinal Colonization and
1139 Transmission of a Bacterial Pathogen. *PLoS Pathog* **11**: e1005107.
1140
- 1141 Sorensen, H.M., Keogh, R.A., Wittekind, M.A., Caillet, A.R., Wiemels, R.E., Laner, E.A.,
1142 and Carroll, R.K. (2020) Reading between the Lines: Utilizing RNA-Seq Data for Global
1143 Analysis of sRNAs in *Staphylococcus aureus*. *mSphere* **5**: e00439-20,
1144 [/msphere/5/4/mSphere439-20.atom](https://doi.org/10.1128/mSphere.00439-20).
1145
- 1146 Tomasini, A., Moreau, K., Chicher, J., Geissmann, T., Vandenesch, F., Romby, P., *et*
1147 *al.* (2017) The RNA targetome of *Staphylococcus aureus* non-coding RNA RsaA:
1148 impact on cell surface properties and defense mechanisms. *Nucleic Acids Research*
1149 **45**: 6746–6760.
1150
- 1151 Trouillet, S., Rasigade, J.-P., Lhoste, Y., Ferry, T., Vandenesch, F., Etienne, J., and
1152 Laurent, F. (2011) A novel flow cytometry-based assay for the quantification of
1153 *Staphylococcus aureus* adhesion to and invasion of eukaryotic cells. *Journal of*
1154 *Microbiological Methods* **86**: 145–149.

- 1155 Villanueva, M., García, B., Valle, J., Rapún, B., Ruiz de los Mozos, I., Solano, C., *et*
1156 *al.* (2018) Sensory deprivation in *Staphylococcus aureus*. *Nat Commun* **9**: 523.
1157
- 1158 Vitko, N.P., Grosser, M.R., Khatri, D., Lance, T.R., and Richardson, A.R. (2016)
1159 Expanded Glucose Import Capability Affords *Staphylococcus aureus* Optimized
1160 Glycolytic Flux during Infection. *mBio* **7**: e00296-16, [/mbio/7/3/e00296-16.atom](https://doi.org/10.1128/mBio.00296-16).
1161
- 1162 Wagner, E.G.H., and Romby, P. (2015) Chapter Three - Small RNAs in Bacteria and
1163 Archaea: Who They Are, What They Do, and How They Do It. In *Advances in Genetics*.
1164 Theodore Friedmann, J.C.D. and S.F.G. (ed.). Academic Press, pp. 133–208
1165 <http://www.sciencedirect.com/science/article/pii/S0065266015000036>. Accessed
1166 August 1, 2016.
1167
- 1168 Wang, C., Chao, Y., Matera, G., Gao, Q., and Vogel, J. (2020) The conserved 3' UTR-
1169 derived small RNA NarS mediates mRNA crossregulation during nitrate respiration.
1170 *Nucleic Acids Research* **48**: 2126–2143.
1171
- 1172 Wencker, F.D.R., Marincola, G., Schoenfelder, S.M.K., Maaß, S., Becher, D., and
1173 Ziebuhr, W. (2021) Another layer of complexity in *Staphylococcus aureus* methionine
1174 biosynthesis control: unusual RNase III-driven T-box riboswitch cleavage determines
1175 *met* operon mRNA stability and decay. *Nucleic Acids Research* **49**: 2192–2212.
1176
- 1177 Wright P.R., Georg J., Mann M., Sorescu D.A., Richter A.S., Lott S., Kleinkauf R., Hess
1178 W.R., Backofen R. (2014) CopraRNA and IntaRNA: predicting small RNA targets,
1179 networks and interaction domains. *Nucleic Acids Res.* **42**: W119-23.
1180
- 1181 Xue, T., You, Y., Hong, D., Sun, H., and Sun, B. (2011) *The Staphylococcus aureus*
1182 KdpDE Two-Component System Couples Extracellular K⁺ Sensing and Agr Signaling
1183 to Infection Programming. *Infect Immun* **79**: 2154–2167.
1184
- 1185 Yang, Y., Sun, H., Liu, X., Wang, M., Xue, T., and Sun, B. (2016) Regulatory
1186 mechanism of the three-component system HptRSA in glucose-6-phosphate uptake in
1187 *Staphylococcus aureus*. *Med Microbiol Immunol* **205**: 241–253.
1188
- 1189
- 1190

1191 **FIGURES LEGENDS**

1192

1193 **Figure 1: RsaG is expressed under *uhpT* promoter activation by HptRS upon**
1194 **sensing external glucose-6-phosphate (G6P).** A. Northern blot analysis of RsaG in
1195 HG001 wild-type strain, HG001 Δ *hptRS* and HG001 Δ *PuhpT*. Total RNA was extracted
1196 at 2, 4 and 6 h of growth in MHB medium with or without the addition of 0.5% G6P. 5S
1197 rRNA (5S) was used as loading control. However, for this control, we used aliquots of
1198 the same RNA preparations but the migration of the samples was performed in parallel
1199 to the experiments on a separate agarose gel because RsaG and 5S rRNA have very
1200 similar sizes. B. Genomic context of *uhpT*-*RsaG* locus and mapping of the different
1201 DNA fragments transcriptionally fused to *gfp* in pCN51 plasmid. Only the full-length
1202 construct carrying the HptR box provided a positive fluorescence signal. The various
1203 sizes of the DNA fragments are given: FL is for full-length, CDS is for coding sequence
1204 of *uhpT*, and 500, 250, and 100 are the number of nucleotides just upstream *rsaG*. C.
1205 Western blot experiment detecting GFP synthesis in the different transcriptional fusion
1206 constructs (FL, CDS, 500, 250, 100) expressed in HG001 wild-type strain. Total
1207 proteins were separated by SDS-PAGE (10%) and were revealed using a GFP-specific
1208 antibody. We used Coomassie staining as loading control. However, we used aliquots
1209 of the same protein preparations, but the migration of the samples was performed in
1210 parallel to the experiments on a separate SDS-PAGE gel.

1211

1212 **Figure 2: The *uhpT* mRNA and RsaG are enhanced under conditions mimicking**
1213 **the infection.** A. Growth curve of HG001 wild-type strain, HG001 Δ *rsaG* and
1214 HG001 Δ *hptRS* strains in LB medium with or without the addition of 0.5% glucose-6-
1215 phosphate (G6P). ns is for non significant, statistical analysis with Anova
1216 (**** $p < 0,0005$). B. Levels of RsaG in HG001 and HG001 Δ *hptRS* strains as determined
1217 with qRT-PCR. Samples were taken after 1 h of *S. aureus* internalization into RAW
1218 264.7 macrophages or CTi400 myoblasts. As control, the yield of RsaG was also
1219 quantified for HG001 wild-type or HG001 Δ *hptRS* cultured for 1 h in K-MEM or D-MEM
1220 medium. Data were normalized to *gyrB* and represent the mean of at least three
1221 independent experiments, **statistical analysis with T-test (* $p < 0,05$)**. C. Left panel,
1222 Northern blot analysis of RsaG in HG001 (pink bars) and HG001 Δ *hptRS* (green bars).
1223 Total RNA was extracted after 1 h incubation with liver cell line Hu-H7 and lung cell
1224 line A549 at days 4 of culture. As control, RNA was extracted from HG001 and

1225 HG001 Δ *hptRS* incubated 1 h in MHB medium supplemented or not with 0.5% glucose-
 1226 6-phosphate (-/+ G6P). Right panel, Mucin 2 (MUC-2) and Mucin 5AC (MUC-5AC)
 1227 proteins were quantified by dot blot assay. 1 μ l of supernatant from the Hu-H7 or A549
 1228 cells incubated with HG001 (pink bars) and HG001 Δ *hptRS* (green bars) were spotted
 1229 on a nitrocellulose membrane. MUC-2 and MUC-5AC were specifically detected with
 1230 anti-MUC-2 or anti-MUC-5AC antibodies. NF: non-infected Hu-H7 or A549 cells.

1231
 1232 **Figure 3: RsaG is matured from *uhpT* by 5'-3' exoribonucleases J1 and J2.** A,
 1233 B. Determination of the 5' end status of various RNAs. 10 μ g of total RNA extracted
 1234 after 4 h of growth in MHB medium (+/- glucose-6-phosphate, G6P) was treated with
 1235 the Terminator™ 5'-Phosphate-Dependent Exonuclease (+/- Tex). **RsaG, 5S (A)** and
 1236 **RsaI (B)** were revealed by Northern blot analysis using specific probes while 5S, 16S
 1237 and 23 rRNAs were visualized by ethidium bromide staining (EtBr) of the agarose gel
 1238 (B). **C.** Northern blot analysis of RsaG in PR02 wild-type strain and PR02-06 (Δ *j1*).
 1239 Total RNA was extracted at 2, 4 and 6 h of growth in MHB medium supplemented with
 1240 10 mg/L uracil and 0.5% glucose-6-phosphate. 5S rRNA (5S) was used as loading
 1241 control (see Figure 1A). **D.** Genomic context of *uhpT*-*RsaG* locus and the sequential
 1242 steps involved in the maturation leading to the accumulation of RsaG. The degradation
 1243 of *uhpT* might involve the RppH enzyme to remove the pyrophosphate although
 1244 RNases J1/J2 can also degrade 5' triphosphate RNA. The 5' hairpin of RsaG blocked
 1245 the progression of the two exoribonucleases leading to its accumulation.

1246
 1247 **Figure 4: RsaG binds to *tcaR*, *sarA* and *ccpA* mRNAs and inhibits their**
 1248 **translation.** A. Secondary structure model of RsaG. The red cytosines have been
 1249 substituted by guanines (in blue) in the RsaG mutants (mut1 or mut2). The predicted
 1250 regions of RsaG complementary to its RNA targets are depicted. On the right side,
 1251 three examples of basepairing interactions are given for *tcaR*, *sarA*, and *ccpA*. The
 1252 Shine and Dalgarno sequences are in bold characters. B. Electrophoretic mobility shift
 1253 assays (EMSA) show the formation of the complex between RsaG and *tcaR*, *sarA*, and
 1254 *ccpA* mRNAs. The 5' end-labeled RsaG was incubated with increasing concentrations
 1255 of cold mRNA (given in nM). C. Toe-print assays showing RsaG effect on the formation
 1256 of the ribosomal initiation complex of *tcaR*, *sarA*, and *ccpA* mRNAs. Lane 1 : incubation
 1257 control of mRNA alone; lane 2 : incubation control of mRNA with 30S subunits; lane 3:
 1258 incubation control of mRNA with RsaG; lane 4 : formation of the ribosomal initiation

1259 complex containing mRNA, 30S and the initiator tRNA^{fMet} (tRNAⁱ); lanes 5 to 8 :
1260 formation of the initiation complex in the presence of increasing concentrations of
1261 RsaG: 50 nM (lane 5), 100 nM (lane 6), 200 nM (lane 7), 400 nM (lane 8) for *tcaR* and
1262 *ccpA*, and 25 nM (lane 5), 100 nM (lane 6), 200 nM (lane 7), 300 nM (lane 8) for *sarA*.
1263 Lanes T, A, C, G: sequencing ladders. The Shine and Dalgarno (SD) sequence, the
1264 start site of translation (ATG) and the toe-printing signals (+16) are indicated.

1265

1266 **Figure 5: Prediction of interaction sites between RsaG and *rex* mRNA.** A.
1267 Secondary structures of RsaG (left) and *rex* mRNA (right). The potential interaction
1268 sites between *rex* and RsaG are named A, B, B', and C. The Shine and Dalgarno
1269 sequence of *rex* and the translational start (AUG) are depicted in green. Substituted
1270 nucleotides in RsaG mut3, mut4 and *rex* R2 are indicated. Below, two possibilities of
1271 interaction schemes between RsaG and *rex* are given with the different sites. B.
1272 Electrophoretic mobility shift assay showing the formation of the complex between
1273 RsaG, RsaG mut3, RsaG mut4 or RsaG mut3/4 and *rex* mRNA. The 5' end-labeled
1274 RsaG or its mutated forms were incubated with increasing concentrations of cold wild-
1275 type *rex* mRNA (*rex*) or of the cold mutant *rex* mRNA carrying R2 substitution (*rex*-R2)
1276 (given in nM). C. Measurements of the half-lives of *rex* mRNA in HG001, HG001Δ*rsaG*
1277 (deletion of *rsaG*) and HG001Δ*rsaG*::pCN51::P3*rsaG* (overexpressing RsaG) strains.
1278 Bacterial cultures were grown in MHB medium containing or not glucose-6-phosphate
1279 (+/- G6P) and treated with rifampicin at 4 h of growth at 37°C. Total RNA was extracted
1280 at various times (from 30 sec to 4 min). RsaG and 5S rRNA were probed to quantify
1281 the yield of RNAs in each lane. Calculated half-lives (normalized to 5S rRNA) are
1282 shown beneath the autoradiography and are the average of two experiments.

1283

1284 **Figure 6: RsaG modulates stability of *ldh1* and *fn3K* mRNAs.** A. EMSA showing
1285 the formation of the complex between RsaG and *ldh1* mRNA. The 5' end-labeled RsaG
1286 was incubated with increasing concentrations of cold mRNA (given in nM). Below the
1287 gels, the predicted interaction site is depicted. The Shine and Dalgarno (SD) sequence
1288 is in bold characters. B. **Electrophoretic mobility shift assay** showing the formation of
1289 the complex between RsaG and *ldh_1* and competition experiment performed with an
1290 oligonucleotide encompassing the region from -14 to +20 of *ldh_1*. The 5' end-labeled
1291 RsaG was incubated with increasing concentrations of cold mRNA (in nM) or with 200
1292 nM of oligonucleotide (Oligo). C. Measurements of the half-lives of *ldh1* and *fn3K* in

1293 wild-type HG001 and mutant HG001 Δ rsaG::pCN51::P3rsaG strains. Bacterial cultures
1294 were grown in MHB medium containing or not glucose-6-phosphate (+/- G6P) treated
1295 with rifampicin at 4 h of growth at 37°C. Total RNA was extracted after 2, 4, 8, and
1296 20 min. Calculated half-lives are shown beneath the autoradiography and are the
1297 average of two experiments (see legend above).

1298

1299 **Figure 7: RsaI affects the binding of several targets to RsaG.** A. Secondary
1300 structure models of RsaG and RsaI. The cytosines in red have been substituted by
1301 guanines (in blue) in the RsaG mutants (mut1 or mut2). The basepairing interactions
1302 between RsaI and RsaG is depicted in the insert. B. Gel retardation assays showing
1303 the formation of the complex between RsaG and RsaI. The 5' end-labeled wild-type
1304 RsaG (RsaG), RsaG mutant 1 (RsaG mut1), RsaG mutant 2 (RsaI mut2), and the
1305 RsaG double mutant 1 and 2 (RsaG mut1/2) were incubated with increasing
1306 concentrations of RsaI (given in nM). C. Ternary complex formation between RsaG,
1307 *sarA* and RsaI. The 5'-end labeled RsaG was incubated with increasing concentrations
1308 of *sarA* mRNA alone or with increasing concentrations of RsaI in the presence of 25
1309 nM of *sarA*. The various complexes are notified on the side of the autoradiography. D.
1310 Complex formation between RsaG, *rex* and RsaI. The 5'-end labeled RsaG was
1311 incubated with increasing concentrations of *rex* mRNA alone or with increasing
1312 concentrations of RsaI in the presence of 150 nM of *rex*. E. Complexes formation
1313 between RsaG, *steT* and RsaI. The 5'-end labeled RsaG was incubated with
1314 increasing concentrations of *steT* mRNA alone or with increasing concentrations of
1315 RsaI in the presence of 150 nM of *steT*. D. Ternary complex formation between RsaG,
1316 *tdcB* and RsaI. The 5'-end labeled RsaG was incubated with increasing concentrations
1317 of *tdcB* mRNA alone or with increasing concentrations of RsaI in the presence of 75
1318 nM of *tdcB*.

1319

1320 **Figure 8: The 3'UTR of *uhpT* mRNA is not conserved in all *staphylococcaceae*.** A.
1321 Genomic context of *uhpT* locus in *Staphylococcus aureus* HG001, *S. argenteus*
1322 MSHR11, *S. schweitzeri* FSA084, *S. epidermidis* ATCC35983 and *S. simiae*
1323 CCM7213T. Percentages given in black represent the similarity score of *uhpT* coding
1324 region and in red the similarity score of *uhpT* 3'UTR compared to *S. aureus*. The
1325 similarity score was obtained by blast (NCBI). B. Northern blot analysis of RsaG in *S.*
1326 *aureus*, *S. argenteus*, *S. schweitzeri*, *S. epidermidis* and *S. simiae*. Total RNA was

1327 extracted at 2, 4 and 6 h of growth in BHI medium containing 0.5% glucose-6-
1328 phosphate (G6P). RsaG from *S. aureus*, *S. argenteus* and *S. schweitzeri* was detected
1329 with a specific probe against *S. aureus* RsaG sequence, while for *S. epidermidis* and
1330 *S. simiae*, the probes were designed against their respective sequences. We used as
1331 internal loading controls, 16S and 23S rRNAs, which were revealed by ethidium
1332 bromide from the same gel. 5S rRNA (5S) was also used as loading control, and was
1333 revealed using a 5' labeled oligonucleotide. However, for this control, we used aliquots
1334 of the same RNA preparations but the migration of the samples was performed in
1335 parallel to the experiments on a separate agarose gel. C. Primer extension performed
1336 on total RNA using a 5'-radiolabeled oligonucleotide complementary to *S. simiae* *uhpT*
1337 3'UTR sequence. Total RNA was extracted from *S. simiae* at 4 h of growth in BHI with
1338 (+) or without (-) 0.5% G6P. The primer is located at nucleotides +108 to +125 (from
1339 the +1 of the putative RsaG). T, C, G, A correspond to sequencing ladders. D. Northern
1340 blot analysis of RsaG in *S. simiae*. Total RNA was extracted at 2, 4 and 6 h of growth
1341 in BHI medium without or with 0.5% G6P. Multiple sequence alignment of the HptR
1342 box in *S. aureus*, *S. argenteus*, *S. schweitzeri*, *S. epidermidis* and *S. simiae* compared
1343 to the consensus sequence underlined in yellow (Yang *et al.*, 2016) using blast (NCBI)
1344 with default settings.

1345

1346 **Figure 9: Model of RsaG regulation networks in *Staphylococcus aureus*.** The two-
1347 component system HptRS is shown in green and the transcriptional regulatory proteins
1348 are in blue. Red bars and arrows are for repression and activation at the post-
1349 transcriptional level, respectively. Black bars and arrows are for repression and
1350 activation at the transcriptional level, respectively. The dotted lines are for the
1351 regulatory mechanisms, which require additional experimental data. The
1352 exoribonuclease activity of RNases J1/J2 is shown in yellow.

1353

1354

1355

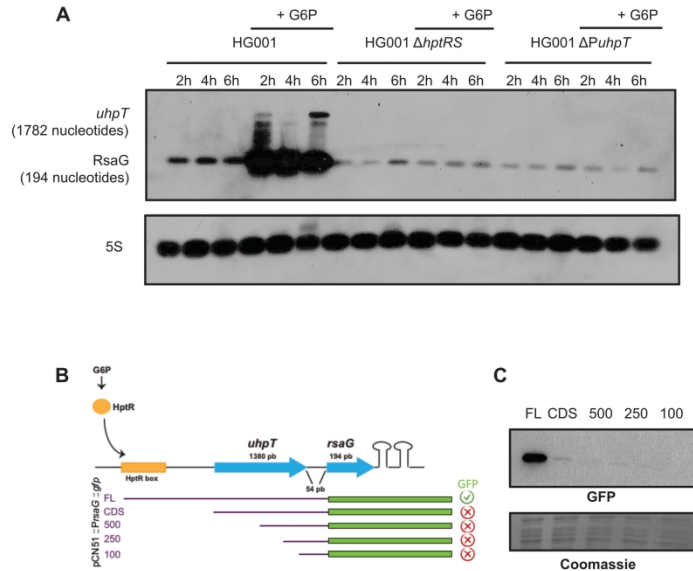


Figure 1

Figure 1: RsaG is expressed under *uhpT* promoter activation by HptRS upon sensing external glucose-6-phosphate (G6P). **A**. Northern blot analysis of RsaG in HG001 wild-type strain, HG001 Δ hptRS and HG001 Δ PuhpT. Total RNA was extracted at 2, 4 and 6 h of growth in MHB medium with or without the addition of 0.5% G6P. 5S rRNA (5S) was used as loading control. However, for this control, we used aliquots of the same RNA preparations but the migration of the samples was performed in parallel to the experiments on a separate agarose gel because RsaG and 5S rRNA have very similar sizes. **B**. Genomic context of *uhpT*-RsaG locus and mapping of the different DNA fragments transcriptionally fused to *gfp* in pCN51 plasmid. Only the full-length construct carrying the HptR box provided a positive fluorescence signal. The various sizes of the DNA fragments are given: FL is for full-length, CDS is for coding sequence of *uhpT*, and 500, 250, and 100 are the number of nucleotides just upstream *rsaG*. **C**. Western blot experiment detecting GFP synthesis in the different transcriptional fusion constructs (FL, CDS, 500, 250, 100) expressed in HG001 wild-type strain. Total proteins were separated by SDS-PAGE (10%) and were revealed using a GFP-specific antibody. We used Coomassie staining as loading control. However, we used aliquots of the same protein preparations, but the migration of the samples was performed in parallel to the experiments on a separate

SDS-PAGE gel.

209x296mm (300 x 300 DPI)

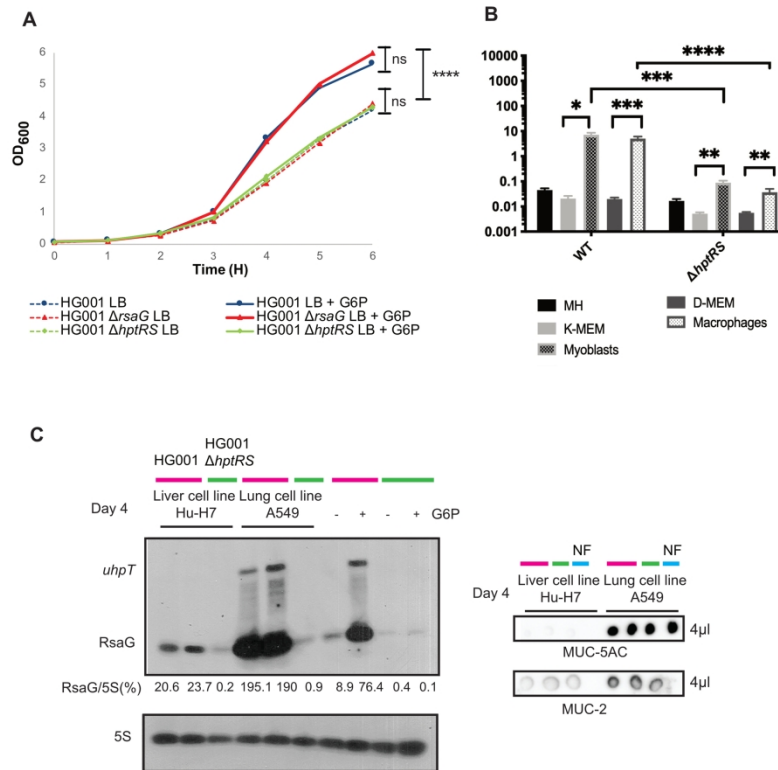


Figure 2

Figure 2: The *uhpT* mRNA and *RsaG* are enhanced under conditions mimicking the infection. A. Growth curve of HG001 wild-type strain, HG001Δ*rsaG* and HG001Δ*hptRS* strains in LB medium with or without the addition of 0.5% glucose-6-phosphate (G6P). ns is for non significant, statistical analysis with Anova (*****p*<0,0005). B. Levels of *RsaG* in HG001 and HG001Δ*hptRS* strains as determined with qRT-PCR.

Samples were taken after 1 h of *S. aureus* internalization into RAW 264.7 macrophages or CTi400 myoblasts. As control, the yield of *RsaG* was also quantified for HG001 wild-type or HG001Δ*hptRS* cultured for 1 h in K-MEM or D-MEM medium. Data were normalized to *gyrB* and represent the mean of at least three independent experiments, statistical analysis with T-test (**p*<0,05). C. Left panel, Northern blot analysis of *RsaG* in HG001 (pink bars) and HG001Δ*hptRS* (green bars). Total RNA was extracted after 1 h incubation with liver cell line Hu-H7 and lung cell line A549 at days 4 of culture. As control, RNA was extracted from HG001 and HG001Δ*hptRS* incubated 1 h in MHB medium supplemented or not with 0.5% glucose-6-phosphate (-/+ G6P). Same legend as in Figure 2C. Right panel, Mucin 2 (MUC-2) and Mucin 5AC (MUC-5AC) proteins were quantified by dot blot assay. 1 μl of supernatant from the Hu-H7 or A549 cells incubated with HG001 (pink bars) and HG001Δ*hptRS* (green bars) were spotted on a nitrocellulose membrane. MUC-2

and MUC-5AC were specifically detected with anti-MUC-2 or anti-MUC-5AC antibodies. NF: non-infected Hu-H7 or A549 cells.

210x297mm (300 x 300 DPI)

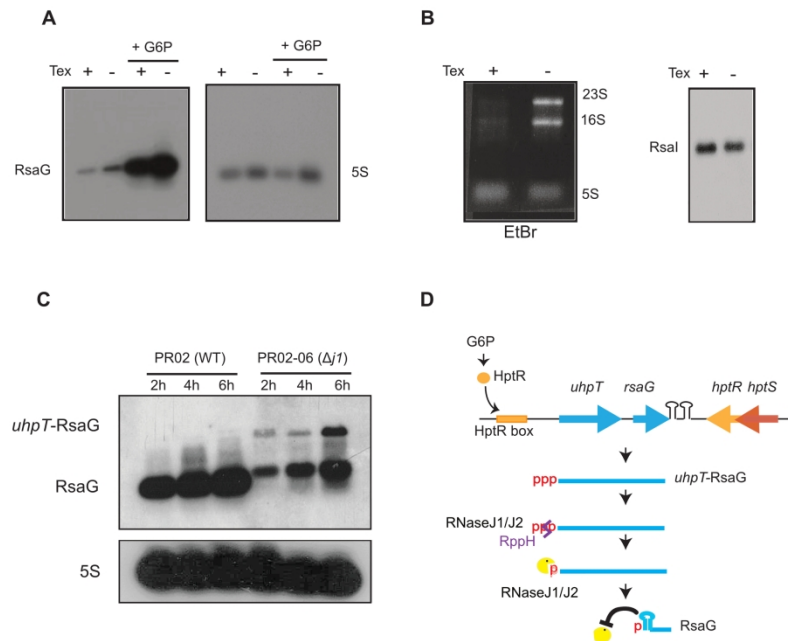


Figure 3

Figure 3: RsaG is matured from *uhpT* by 5'-3' exoribonucleases J1 and J2. A, B. Determination of the 5' end status of various RNAs. 10 μ g of total RNA extracted after 4 h of growth in MHB medium (+/- glucose-6-phosphate, G6P) was treated with the Terminator™ 5'-Phosphate-Dependent Exonuclease (+/- Tex). RsaG, 5S (A) and RsaI (B) were revealed by Northern blot analysis using specific probes while 5S, 16S and 23 rRNAs were visualized by ethidium bromide staining (EtBr) of the agarose gel (B). C. Northern blot analysis of RsaG in PR02 wild-type strain and PR02-06 ($\Delta j1$). Total RNA was extracted at 2, 4 and 6 h of growth in MHB medium supplemented with 10 mg/L uracil and 0.5% glucose-6-phosphate. 5S rRNA (5S) was used as loading control (see above). D. Genomic context of *uhpT*-RsaG locus and the sequential steps involved in the maturation leading to the accumulation of RsaG. The degradation of *uhpT* involves most probably the RppH enzyme to remove the pyrophosphate subsequently followed by the attack of RNases J1/J2. The 5' hairpin of RsaG blocked the progression of the two exoribonucleases leading to its accumulation.

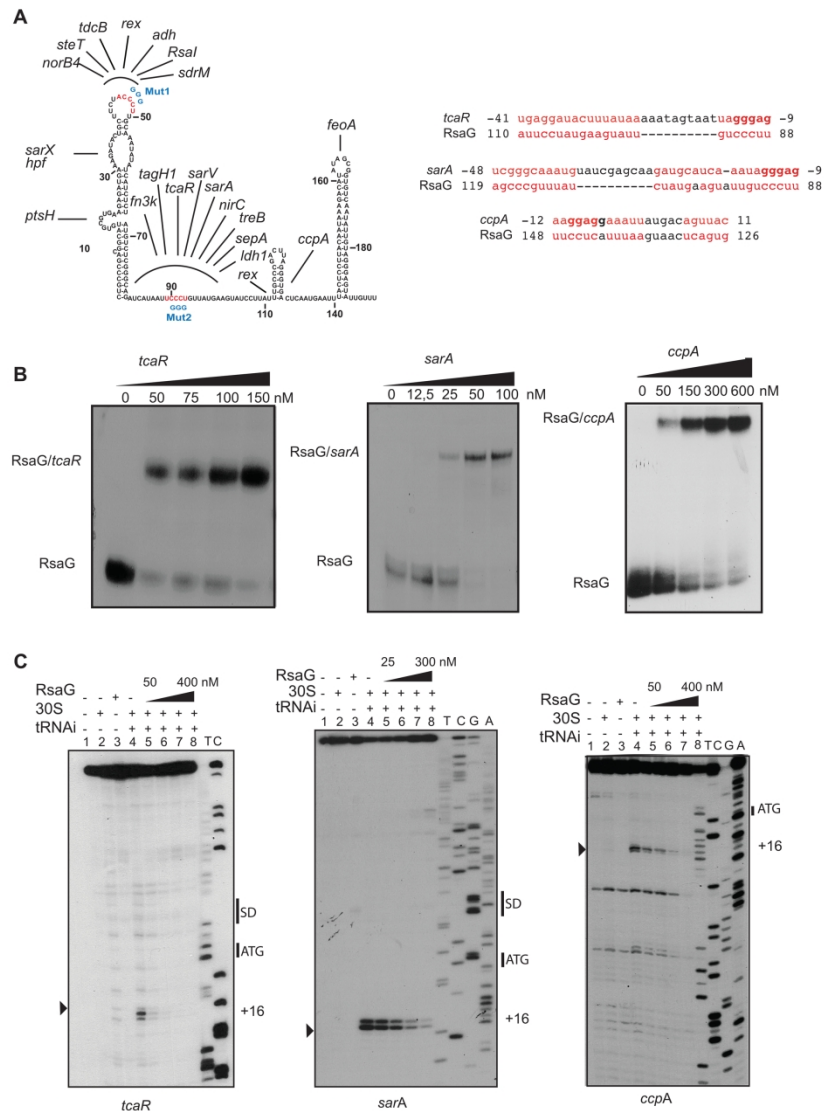


Figure 4

Figure 4: RsaG binds to *tcaR*, *sarA* and *ccpA* mRNAs and inhibits their translation.

A. Secondary structure model of RsaG. The red cytosines have been substituted by guanines (in blue) in the RsaG mutants (mut1 or mut2). The predicted regions of RsaG complementary to its targets are depicted. On the right side, three examples of basepairing interactions are given for *tcaR*, *sarA*, and *ccpA*. The translation start codon sequence is underlined, and Shine and Dalgarno (SD) sequences are in bold characters. B.

Electrophoretic mobility shift assays (EMSA) show the formation of the complex between RsaG and *tcaR*, *sarA*, and *ccpA* mRNAs. The 5' end-labeled RsaG was incubated with increasing concentrations of cold mRNA (given in nM). C. Toe-print assays showing RsaG effect on the formation of the ribosomal initiation complex of *tcaR*, *sarA*, and *ccpA* mRNAs. Lane 1 : incubation control of mRNA alone; lane 2 : incubation control of mRNA with 30S subunits; lane 3: incubation control of mRNA with RsaG; lane 4 : formation of the ribosomal initiation complex containing mRNA, 30S and the initiator tRNA^{fMet} (tRNAⁱ); lanes 5 to 8 : formation of the initiation complex in the presence of increasing concentrations of RsaG: 50 nM (lane 5), 100 nM (lane 6), 200 nM (lane 7), 400 nM (lane 8) for *tcaR* and *ccpA*, and 150 nM (lane 6), 300 nM (lane 7) for *sarA*. Lanes T, A, C, G: sequencing ladders. The Shine and Dalgarno (SD) sequence, the start site of translation (ATG)

and the toe-printing signals (+16) are indicated.

209x296mm (300 x 300 DPI)

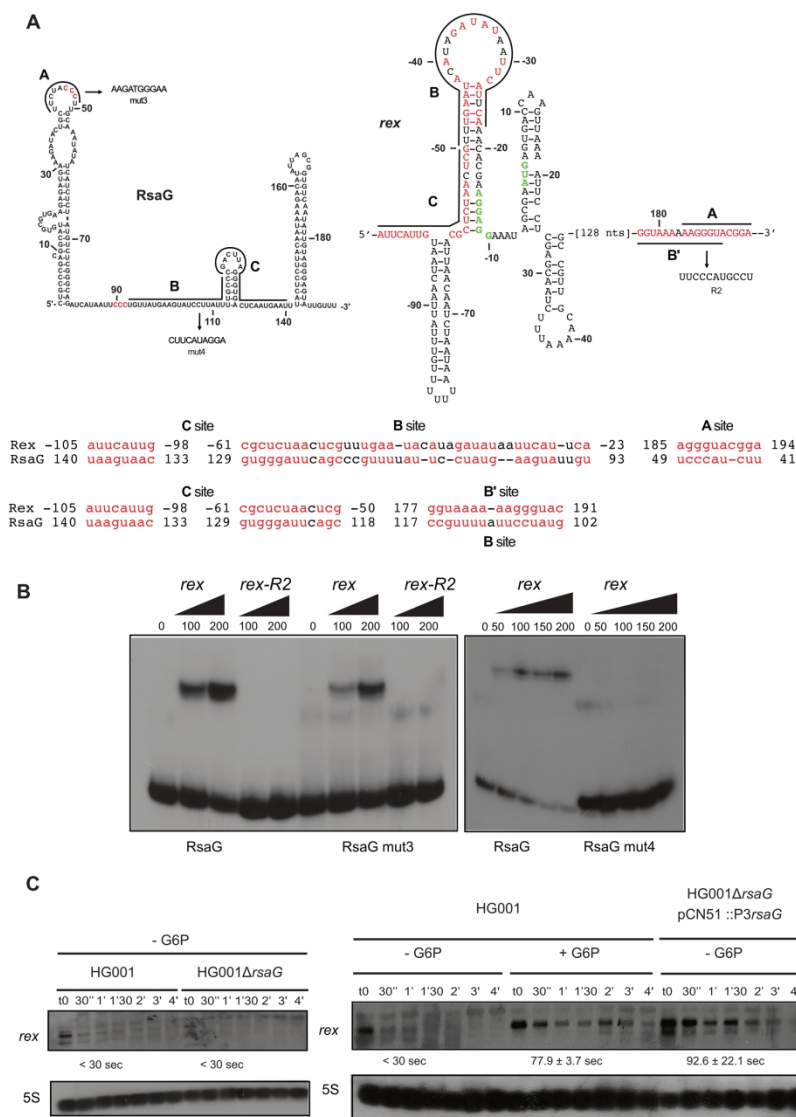


Figure 5

Figure 5: Prediction of interaction sites between RsaG and rex mRNA. A. Secondary structures of RsaG (left) and rex mRNA (right). The potential interaction sites between rex and RsaG are named A, B, B', and C. The Shine and Dalgarno sequence of rex and the translational start (AUG) are depicted in green. Substituted nucleotides in RsaG mut3, mut4 and rex R2 are indicated. Below, two possibilities of interaction schemes between RsaG and rex are given with the different sites. B. Electrophoretic mobility shift assay showing the formation of the complex between RsaG, RsaG mut3, RsaG mut4 or RsaG mut3/4 and rex mRNA. The 5' end-labeled RsaG or its mutated forms were incubated with increasing concentrations of cold wild-type rex mRNA (rex) or of the cold mutant rex mRNA carrying R2 substitution (rex-R2) (given in nM). C.

Measurements of the half-lives of rex mRNA in HG001, HG001ΔrsaG (deletion of rsaG) and HG001ΔrsaG::pCN51::P3rsaG (overexpressing RsaG) strains. Bacterial cultures were grown in MHB medium containing or not glucose-6-phosphate (+/- G6P) and treated with rifampicin at 4 h of growth at 37°C. Total RNA was extracted at various times (from 30 sec to 4 min). RsaG and 5S rRNA were probed to quantify the yield of RNAs in each lane. Calculated half-lives (normalized to 5S rRNA) are shown beneath the autoradiography and are the average of two experiments.

209x296mm (300 x 300 DPI)

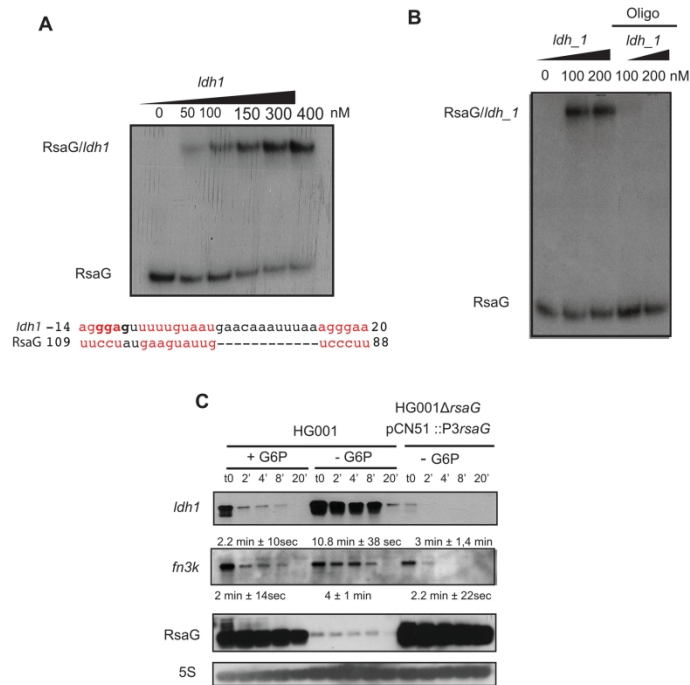


Figure 6

Figure 6: RsaG modulates stability of *ldh1* and *fn3K* mRNAs.

A. EMSA showing the formation of the complex between RsaG and *ldh1* mRNA. The 5' end-labeled RsaG was incubated with increasing concentrations of cold mRNA (given in nM). Below the gels, the predicted interaction site is depicted. The Shine and Dalgarno (SD) sequence is in bold characters. B. EMSA showing the formation of the complex between RsaG and *ldh_1* and competition experiment performed with an oligonucleotide encompassing the region from -14 to +20 of *ldh_1*. The 5' end-labeled RsaG was incubated with increasing concentrations of cold mRNA (in nM) or with 200 nM of oligonucleotide (Oligo). C. Measurements of the half-lives of *ldh1* and *fn3K* in HG001 and HG001Δ*rsaG*::pCN51::P3*rsaG* strains. Bacterial cultures were grown in MHB medium containing or not glucose-6-phosphate (+/- G6P) treated with rifampicin at 4 h of growth at 37°C. Total RNA was extracted after 2, 4, 8 and 20 min. Calculated half-lives are shown beneath the autoradiography and are the average of two experiments.

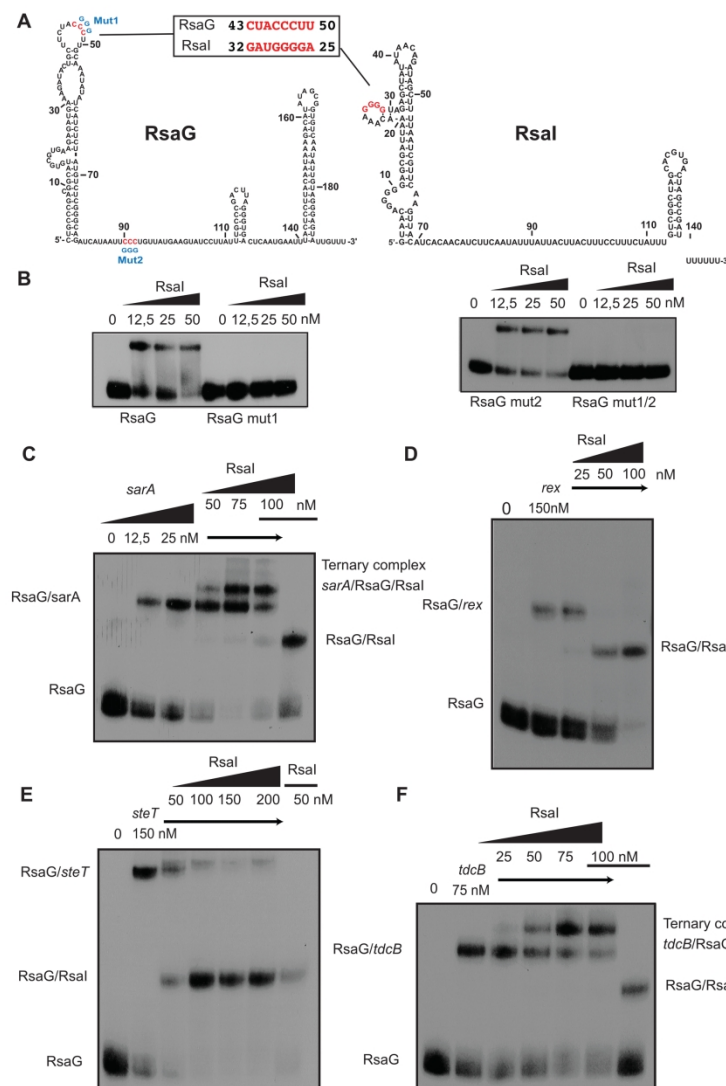


Figure 7

Figure 7: RsaI affects only part of the regulatory functions of RsaG. A. Secondary structure models of RsaG and RsaI. The cytosines in red have been substituted by guanines (in blue) in the RsaG mutants (mut1 or mut2). The basepairing interactions between RsaI and RsaG are depicted. B. Gel retardation assays showing the formation of the complex between RsaG and RsaI. The 5' end-labeled wild-type RsaG (RsaG), RsaG mutant 1 (RsaG mut1), RsaG mutant 2 (RsaI mut2), and the RsaG double mutant 1 and 2 (RsaG mut1/2) were incubated with increasing concentrations of RsaI (given in nM). C. Ternary complex formation between RsaG, *sarA* and RsaI. The 5'-end labeled RsaG was incubated with increasing concentrations of *sarA* mRNA alone or with increasing concentrations of RsaI in the presence of 25 nM of *sarA*. The various complexes are notified on the side of the autoradiography. D. Complex formation between RsaG, *rex* and RsaI. The 5'-end labeled RsaG was incubated with increasing concentrations of *rex* mRNA alone or with increasing concentrations of RsaI in the presence of 150 nM of *rex*. E. Complexes formation between RsaG, *steT* and RsaI. The 5'-end labeled RsaG was incubated with increasing concentrations of *steT* mRNA alone or with increasing concentrations of RsaI in the presence of 150 nM of *steT*. D. Ternary complex formation between RsaG, *tdcB* and RsaI. The 5'-end labeled RsaG was incubated with increasing concentrations of *tdcB* mRNA

alone or with increasing concentrations of RsaI in the presence of 75 nM of tdcB.

209x296mm (300 x 300 DPI)

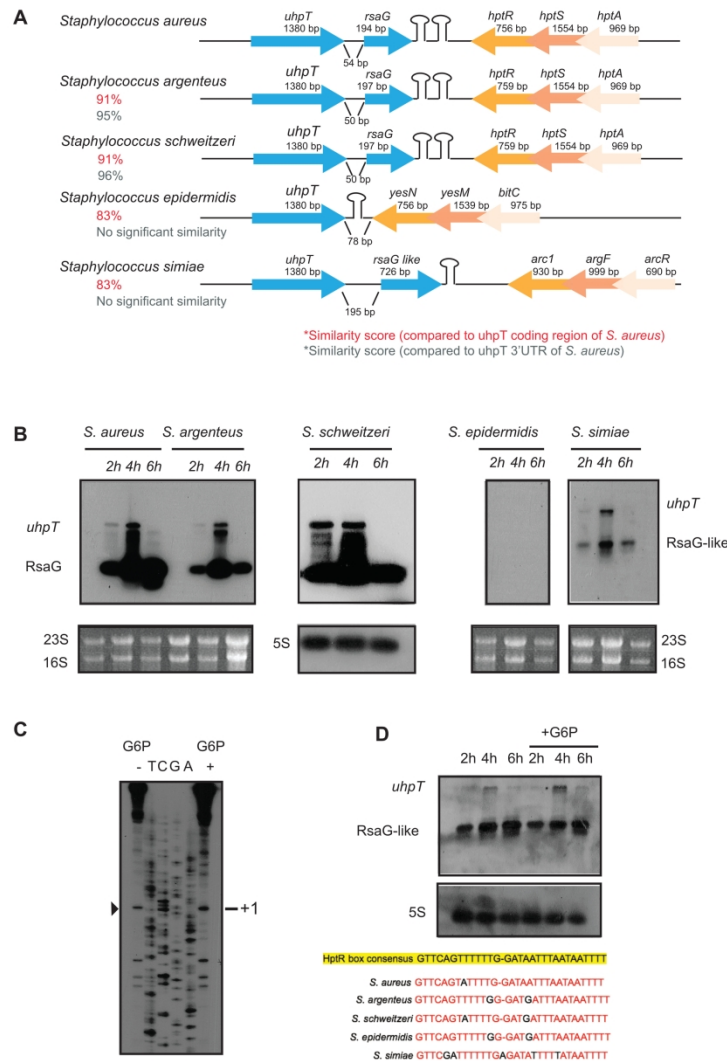


Figure 8

Figure 8: The 3'UTR of *uhpT* mRNA is not conserved in all staphylococcaceae. A. Genomic context of *uhpT* locus in *Staphylococcus aureus* HG001, *S. argenteus* MSHR11, *S. schweitzeri* FSA084, *S. epidermidis* ATCC35983 and *S. simiae* CCM7213T. Percentages given in black represent the similarity score of *uhpT* coding region and in red the similarity score of *uhpT* 3'UTR compared to *S. aureus*. The similarity score was obtained by blast (NCBI). B. Northern blot analysis of RsaG in *S. aureus*, *S. argenteus*, *S. schweitzeri*, *S. epidermidis* and *S. simiae*. Total RNA was extracted at 2, 4 and 6 h of growth in BHI medium containing 0.5% glucose-6-phosphate (G6P). RsaG from *S. aureus*, *S. argenteus* and *S. schweitzeri* was detected with a specific probe against *S. aureus* RsaG sequence, while for *S. epidermidis* and *S. simiae*, the probes were designed against their respective sequences. We used as internal loading controls, 16S and 23S rRNAs, which were revealed by ethidium bromide from the same gel. 5S rRNA (5S) was also used as loading control, and was revealed using a 5' labeled oligonucleotide. However, for this control, we used aliquots of the same RNA preparations but the migration of the samples was performed in parallel to the experiments on a separate agarose gel. C. Primer extension performed on total RNA using a 5'-radiolabeled oligonucleotide complementary to *S. simiae* *uhpT* 3'UTR sequence. Total RNA was extracted from *S. simiae*

at 4 h of growth in BHI with (+) or without (-) 0.5% G6P. The primer is located at nucleotides +108 to +125 (from the +1 of the putative RsaG). T, C, G, A correspond to sequencing ladders. D. Northern blot analysis of RsaG in *S. simiae*. Total RNA was extracted at 2, 4 and 6 h of growth in BHI medium without or with 0.5% G6P. Multiple sequence alignment of the HptR box in *S. aureus*, *S. argenteus*, *S. schweitzeri*, *S. epidermidis* and *S. simiae* compared to the consensus sequence underlined in yellow (Yang et al., 2016) using blast (NCBI) with default settings.

209x296mm (300 x 300 DPI)

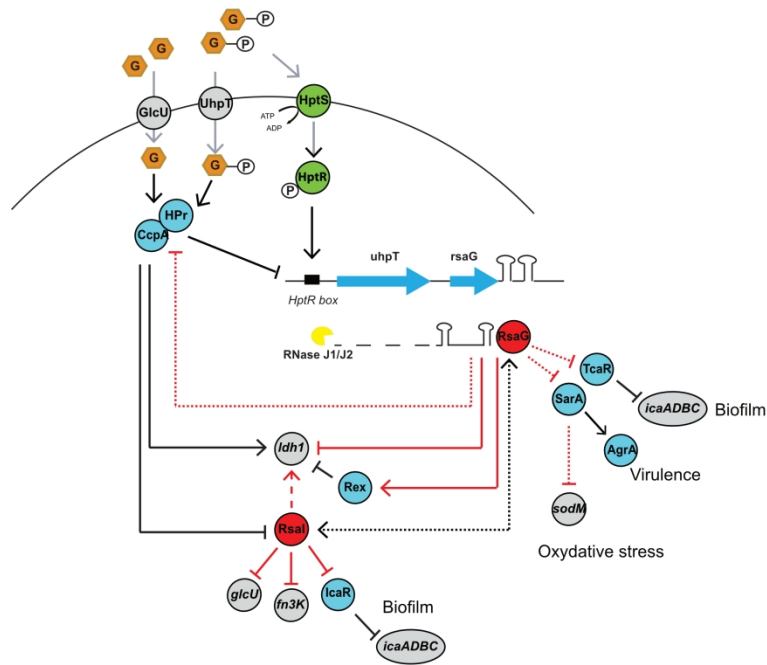
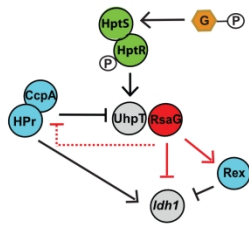


Figure 9

Figure 9: Model of RsaG regulation networks in *Staphylococcus aureus*. The two-component system HptRS is shown in green and the transcriptional regulatory proteins are in blue. Red bars and arrows are for repression and activation at the post-transcriptional level, respectively. Black bars and arrows are for repression and activation at the transcriptional level, respectively. The dotted lines are for the regulatory mechanisms, which require additional experimental data. The exoribonuclease activity of RNases J1/J2 is shown in yellow.



RsaG is a 3'UTR derived regulatory RNA issued from the degradation of the *uhpT* transcript encoding the glucose-6-phosphate (G6P) transporter in *Staphylococcus aureus*. In presence of G6P, sensed by HptRS, RsaG would transiently favour G6P entry by repressing CcpA-Hpr synthesis. Accordingly, it modulates the redox homeostasis by stabilizing *rex* and degrading *ldh1* mRNAs. The regulation is particularly important when *S. aureus* is in contact of mucus-secreting cells or when it is internalised into host cells.

For Peer Review